Published in final edited form as:

Neuron. 2018 September 05; 99(5): 941–955.e4. doi:10.1016/j.neuron.2018.07.026.

Timing mechanisms underlying gate control by feedforward inhibition

Yan Zhang[1,2,3,4], **Shenbin Liu**[1,5], **Yu-Qiu Zhang**[5], **Martyn Goulding**[6], **Yan-Qing Wang**[2,3,5,*], and **Qiufu Ma**[1,7,**]

[1]Dana-Farber Cancer Institute and Department of Neurobiology, Harvard Medical School, Boston, MA 02115, USA.

[2]Institute of Acupuncture and Moxibustion, Fudan Institutes of Integrative Medicine, Shanghai, 200032, China.

[3]Department of Integrative Medicine and Neurobiology, School of Basic Medical Science; Fudan University, Shanghai, 200032, China.

[4]Cell Electrophysiology Laboratory, Wannan Medical College, Wuhu, 241002, China.

[5]Institute of Brain Science, the State Key Laboratory of Medical Neurobiology and the Collaborative Innovation Center for Brain Science, Fudan University, Shanghai, 200032, China.

[6]Molecular Neurobiology Laboratory, The Salk Institute for Biological Studies, 10010 North Torrey Pines Road, La Jolla, CA 92037, USA.

[7]Lead Contact

SUMMARY

The gate control theory proposes that Aβ mechanoreceptor inputs to spinal pain transmission T neurons are gated via feedforward inhibition, but it remains unclear how monosynaptic excitation is gated by di-synaptic inhibitory inputs that arrive later. Here we report that Aβ-evoked non-NMDAR-dependent EPSPs in T neurons are subthreshold, allowing time for inhibitory inputs to prevent action potential firing that requires slow-onset NMDAR activation. Potassium channel activities, including I_A whose sizes are established constitutively by Preprodynorphin^{Cre}-derived inhibitory neurons, either completely filter away Aβ inputs or make them subthreshold, thereby creating a permissive condition to achieve gate control. Capsaicin-activated nociceptor inputs reduce I_A and sensitize the T neurons, allowing Aβ inputs to cause firing before inhibitory inputs arrive. Thus, distinct kinetics of glutamate receptors and electric filtering by potassium channels solve the timing problem underlying the gating by feedforward inhibition, and their modulation offers a way to bypass the gate control.

*Correspondence: wangyanqing@shmu.edu.cn. **Correspondence: Qiufu_Ma@dfci.harvard.edu (Q.M.).

AUTHOR CONTRIBUTIONS

Conceptualization, Y.Z., Q.M., and Y.-Q.W; Methodology, Y.Z., S.L., Q.M., and M.G.; Investigation and formal analysis, Y.Z. and B.L.; Writing-Original Draft, Y.Z. and Q.M.; Writing-Review & Editing, Y.Z., Q.M., S.L., Y.-Q.W., Y.-Q.Z and M.G; Funding acquisition: Y.Z., Q.M., S.L., Y.-Q.W., Y.-Q.Z and M.G.; Resources, M.G.; Supervision: Q.M., Y.-Q.W., and Y.-Q.Z.

DECLARATION OF INTERESTS

The authors declare no competing interests

In Brief:

Zhang et al. uncover a timing mechanism allowing monosynaptic excitation gated by di-synaptic feedforward inhibition, involving with glutamate receptor kinetics and dendritic electric filtering by potassium channels.

INTRODUCTION

The “gate control theory” (GCT) of pain was first postulated by Melzack and Wall in 1965 (Melzack and Wall, 1965), and has since been revised (Braz et al., 2014; Mendell, 2014). The theory suggests the convergent inputs to the spinal cord transmission (“T”) neurons from small-diameter primary afferents that include unmyelinated C-fiber nociceptors (Bessou and Perl, 1969), and from large-diameter primary afferents, which include myelinated Aβ low threshold mechanoreceptors (Figure 1A). The GCT contains two key tenets. The first is that activation of Aβ afferents establishes a gate by feedforward activation of inhibitory interneurons (INs), which acts to attenuate excitatory inputs to T neurons from Aβ and C fibers; as such, under normal conditions, innocuous mechanical stimuli fail to activate T neurons and to evoke pain. The other tenet states that the gate can be opened by “inactivating” INs following strong inputs from C fibers and thinly myelinated Aδ fibers, which in turn allows primary afferents to drive sufficient inputs to activate T neurons. Recent studies have revealed multiple gated spinal pathways that relay Aβ inputs to presumptive T neurons (Baba et al., 2003; Cheng et al., 2017; Cui et al., 2016; Duan et al., 2018; Duan et al., 2014; Lu et al., 2013; Peirs et al., 2015; Petitjean et al., 2015; Torsney and MacDermott, 2006). One such population of T neurons is marked genetically by the expression of Somatostatin-Cre (SOM^{Cre}). These neurons include vertical cells that send dendrites to laminae III/IV and receive direct Aβ inputs, and this direct pathway is gated by inhibitory neurons marked by the expression of preprodynorphin-Cre ($Pdyn^{Cre}$) (Duan et al., 2014). T neurons also receive polysynaptic Aβ inputs that start with excitatory interneurons located in lamina III (Baba et al., 2003; Cheng et al., 2017; Duan et al., 2014; Lu et al., 2013; Peirs et al., 2015; Torsney and MacDermott, 2006), and Aβ inputs to these interneurons are gated by a series of molecularly and genetically marked inhibitory neurons (Cui et al., 2016; Duan et al., 2014; Lu et al., 2013; Petitjean et al., 2015).

Several key questions remain. First, from the point of view of timing, how can T neurons receiving monosynaptic Aβ excitatory inputs be gated by the delayed arrival of di-synaptic inhibitory inputs? Second, it also remains poorly understood on how strong C fiber inputs overcome this gate control (Figure 1A). Take intradermal capsaicin injection as an example. Capsaicin activates nociceptors expressing the transient potential receptor V1 (TRPV1) (Julius, 2013) and its intradermal injection is able to open the gate, leading to the manifestation of mechanical allodynia-pain evoked by innocuous tactile stimuli (Koltzenburg et al., 1992; Torebjork et al., 1992), as any injury-causing stimuli do (Lewis, 1936). However, it remains unclear whether capsaicin-evoked inputs really inactivate the inhibitory gate as predicted by GCT (Figure 1A). Here we found that the kinetics of different glutamate receptors and dendritic electric filtering by potassium channels, including I_A currents, jointly solve the timing problem. We then show that the sizes of I_A currents depend on the constitutive activity of $Pdyn^{Cre}$-derived inhibitory neurons, and capsaicin-evoked

nociceptor inputs overcame the gate control, partly via attenuation of I_A currents, rather than a direct silencing of inhibitory neurons. Along the way, we discovered massive "silent" Aβ inputs to superficial dorsal horn neurons caused by strong electric filtering along the dendrites to the soma.

RESULTS

Capsaicin-induced mechanical hypersensitivity depends on SOM^{Cre}-derived spinal neurons

In this study we set out to understand the timing mechanisms associated with spinal gate control under normal conditions and gate opening following nociceptor activation, using hindpaw capsaicin injection as a model (Figure 1A). We first characterized the spinal circuits that are sensitized by capsaicin. Since SOM^{Cre}-derived neurons are required to transmit mechanical allodynia induced by inflammation and nerve injury (Duan et al., 2014), we examined how capsaicin-evoked allodynia was affected in mice with selective ablation of spinal SOM^{Lbx1} neurons defined by coexpression of SOM^{Cre} and $Lbx1^{Flpo}$, using the intersectional genetic strategy we developed recently (Bourane et al., 2015b; Cheng et al., 2017; Duan et al., 2014). Following intraplantar capsaicin injection, SOM^{Lbx1}-ablated mice displayed acute licking behavior, with licking times comparable to control littermates (control, n=8, 30.1 ± 4.0 s; ablation, n=6, 26.1 ± 4.5 s; two-tailed Student's unpaired test, $p = 0.506$). Following capsaicin injection, control littermates developed: 1) punctate mechanical hypersensitivity, as indicated by reduced withdrawal thresholds in response to von Frey filament stimulation and 2) brush-evoked dynamic hypersensitivity, as measured by the scoring system we reported recently (Figure 1B) (Cheng et al., 2017; Duan et al., 2014). Both forms of hypersensitivity were largely abolished in SOM^{Lbx1}-ablated mice (Figure 1B).

Capsaicin-induced dynamic allodynia is mediated via Aβ fibers in humans (Koltzenburg et al., 1992; Torebjork et al., 1992). Upon developing allodynia, Aβ inputs are relayed from laminae III-V to lamina I and the outer layer of lamina II (I-II_o) via multiple pathways (Duan et al., 2018), where a subset of pain output neurons is located (Todd, 2010). We therefore performed whole-cell patch clamp recordings of neurons in I-II_o. In untreated control mice, voltage clamp recordings with the membrane potential held at −70 mV showed that 50% (22 of 44) of neurons in I-II_o produced EPSCs (Excitatory Postsynaptic Currents) following electric stimulation at intensity (25 μA) that selectively activated Aβ afferents (Duan et al., 2014). Current clamp recordings showed that most evoked excitatory postsynaptic potentials (eEPSPs) were subthreshold, with only 9% (4 of 44) of I-II_o neurons firing action potentials (APs) (Figure 1C). In capsaicin-injected control littermates, the percentage of neurons displaying Aβ-evoked EPSCs (Aβ-eEPSCs) and APs (Aβ-eAPs) increased to 88% (21 of 24, Chi-square test, $p < 0.01$) and 54% (13 of 24, Chi-square test, $p < 0.001$), respectively (Figure 1C). In capsaicin-injected SOM^{Lbx1}-ablated mice, Aβ-eEPSCs and Aβ-eAPs were reduced to 42% (14 of 33, Chi-square test, $p < 0.001$) and 9% (3 of 33, Chi-square test, $p < 0.001$), respectively (Figure 1C). SOM^{Cre}-derived neurons are therefore required for the transmission of sensitized Aβ inputs to the superficial dorsal horn.

Capsaicin injection mainly sensitized SOM^{Cre}-negative neurons

Our findings that the SOM^{Cre}-derived neurons are dispensable for capsaicin-induced acute licking responses, but essential for the expression of mechanical hypersensitivity raised the question as to how SOM^{Cre}-derived and SOM^{Cre}-negative neurons respond to Aβ stimulation. *SOM$^{Cre/+}$* mice were crossed with ai14 tdTomato reporter mice to mark SOM^{Cre}-derived neurons. We first focused on the lamina II and III border, referred to as $_{v}$II$_{i}$-$_{d}$III for the region covering the most ventral portion of the inner lamina II ($_{v}$II$_{i}$) and the most dorsal part of lamina III ($_{d}$III). Under naïve conditions, 20% (3 of 15) of SOM^{Cre}-tdTomato^{+} neurons in $_{v}$II$_{i}$-$_{d}$III fired APs, which we referred to as type I cells (Duan et al., 2014); capsaicin injection did not cause significant change in the percentage of these cells with AP firing (24%, 8 of 33, Chi-square test, p = 1.000). For SOM^{Cre}-tdTomato^{+} neurons in I-II$_{o}$, none (0 of 26) of them generated Aβ-eAPs under naïve conditions (Figure 1D). Upon capsaicin injection, 15% fired APs (5 out 34, Chi-square test, $p < 0.05$) (Figure 1D). SOM^{Cre}-tdTomato^{+} neurons only represent 8.3% (8/96) of recorded neurons in these superficial laminae. In other words, among 45% of neurons in I-II$_{o}$ gaining Aβ-eAPs after capsaicin treatment, SOM^{Cre}-tdTomato^{+} cells only account for 2.7% (15% × 8.3% / 45%).

We then examined SOM^{Cre}-tdTomato-negative neurons in I-II$_{o}$, and observed a marked increase in the percentage receiving Aβ-eEPSCs, from 53% (21 of 40) in naïve mice to 91% (30 of 33, Chi-square test, $p < 0.001$) following capsaicin injection. Current clamp recordings showed that neurons with Aβ eAPs increased by 57%, from 10% (4 of 40) to 67% (22 of 33, Chi-square test, $p < 0.001$) (Figure 1E). Within $_{v}$II$_{i}$-$_{d}$III, there was also a marked increase of SOM^{Cre}-negative neurons with Aβ-eEPSCs, from 55% (16 of 29) in naive mice to 88% following capsaicin treatment (30 of 34, Chi-square test, $p < 0.01$). The same is true for neurons producing Aβ eAPs, from 10% (3 of 29) to 56% (19 of 34, Chi-square test, $p < 0.001$), a 46% increase (Figure 1F). Thus, capsaicin injection sensitizes a large subset of SOM^{Cre}-negative neurons located in I-II$_{o}$ and $_{v}$II$_{i}$-$_{d}$III, plus a very small subset of SOM^{Cre}-derived neurons located in I-II$_{o}$. We next assessed whether recorded neurons received monosynaptic Aβ inputs or not, based on their ability to follow high frequency stimulation with constant latency, as we defined previously (Cheng et al., 2017). Among neurons with Aβ-evoked APs after capsaicin treatment, monosynaptic inputs occur in 74% (14 of 19) of SOM^{Cre}-negative neurons in $_{v}$II$_{i}$-$_{d}$III (Figure 1F); however, in I-II$_{o}$, only 20% (1 of 5) of SOM^{Cre}-tdTomato^{+} neurons and 23% (5 of 22) of Som^{Cre}-negative neurons receive monosynaptic inputs, indicating the involvement of interneurons linking Aβ inputs to superficial dorsal horn neurons.

What are the identities of SOM^{Cre}-negative neurons sensitized by capsaicin? SOM^{Cre}-derived spinal neurons are predominantly glutamatergic excitatory neurons (Duan et al., 2014; Gutierrez-Mecinas et al., 2016). We first assessed the whole population of spinal inhibitory neurons marked by developmental VGAT^{Cre} expression (Vong et al., 2011), and found that the percentage of these neurons with Aβ eAPs increased by 33%, from 30% (7/23) in control to 63% (12/19) after capsaicin treatment (Chi-square test, $p < 0.05$) (Figure S1). Inhibitory neurons account for less than 30% of neurons in laminae I and II (Polgar et al., 2003; Polgar et al., 2013), and we accordingly estimated that among 45% (54% - 9%) I-II$_{o}$ neurons sensitized by capsaicin with Aβ eAPs (Fig. 1C), only ~10% (33% × 30%)

belong to inhibitory neurons; the remaining 35% are excitatory, accounting for half of all excitatory neurons [35% / (100%- 30%) = 50%]. Other studies show that only 5–10% of lamina I neurons send ascending projections to brain (Spike et al., 2003; Cameron et al., 2015), indicating that a majority of I-II$_o$ neurons sensitized by capsaicin are interneurons. We then assessed VGLUT3^{Cre}-derived spinal interneurons, which are required to mediate dynamic allodynia induced by nerve injury or inflammation (Cheng et al., 2017). Following capsaicin treatment, only 4.5% (1/22) of recorded VGLUT3^{Cre}-tdTomato$^+$ neurons producing Aβ eAPs, which is not different from 2.5% (3/119) seen in naïve mice (Cheng et al., 2017) (Chi-square test, p = 0.599). Accordingly, capsaicin-induced dynamic allodynia remained intact in VGLUT3^{Lbx1}-ablated mice (Figure S2). Thus, besides 33% of inhibitory neurons, capsaicin sensitizes ~50% of excitatory neurons in I-II$_o$ that are predominantly double negative for SOM^{Cre} and VGLUT3^{Cre}.

Since capsaicin-induced Aβ inputs to neurons in I-II$_o$ were lost in SOM^{Lbx1}-ablated mice (Figure 1C), there must be interconnections between SOM^{Cre}-tdTomato$^+$ and SOM^{Cre}-negative neurons (Figure 1G). For sensitized SOM^{Cre}-tdTomato$^+$ neurons in I-II$_o$ with indirect Aβ inputs, they might receive inputs from sensitized SOM^{Cre}/VGLUT3^{Cre}-negative neurons located in $_v$II$_i$-$_d$III (Figure 1G, Pathway 1). For sensitized SOM^{Cre}/VGLUT3^{Cre}-negative neurons in I-II$_o$, they might receive inputs from type 1 SOM^{Cre}-tdTomato$^+$ neurons in $_v$II$_i$-$_d$III that normally produce Aβ eAPs (Duan et al., 2014), so as to explain the loss of such inputs in SOM^{Lbx1}-ablated mice (Figure 1G, Pathway 2).

Timing mechanisms underlying gate control at the II-III border

Since capsaicin injection predominantly sensitizes the SOM^{Cre}-negative neurons, we focused on these neurons for subsequent gate control studies. We first studied SOM^{Cre}-negative neurons in $_v$II$_i$-$_d$III; as shown above (Figure 1F), 55% of them receive Aβ-eEPSCs without AP firing under naïve conditions. To determine if the lack of AP firing was due to feedforward inhibition, we performed recordings in the presence of bicuculline (10 μM) and strychnine (2 μM), which block inhibitory GABA$_A$ receptors and glycine receptors, respectively. Under this disinhibition condition, 100% (14 of 14) of these neurons fired APs (Figure 2B), in comparison with 10% under normal conditions (Chi-square test, p < 0.001) (Figure 1F). As shown in Figure 1F, a majority of SOM^{Cre}-negative neurons in $_v$II$_i$-$_d$III received monosynaptic Aβ inputs, raising the timing question on how they could be gated by di-synaptic or even poly-synaptic inhibitory inputs. To address this question, we measured latencies of Aβ-eEPSCs, eIPSCs (evoked inhibitory postsynaptic currents) and eAPs under normal or disinhibition conditions. To facilitate the recording of Aβ-eIPSCs (Aβ-eIPSCs), the membrane potential was held at 0 mV to minimize the interference by eEPSCs (Yoshimura and Jessell, 1990), even though IPSCs could still be produced in spines and/or distal dendrites due to voltage clamp failure (Armstrong and Gilly, 1992; Beaulieu-Laroche and Harnett, 2018; Williams and Mitchell, 2008). QX-314 (5 mM), a membrane-impermeable sodium channel blocker (Binshtok et al., 2007), was included in the recording electrode. At this concentration, QX-314 blocked AP firing following current injection (data not shown). Using this recording method, we found that the mean latency of Aβ-eIPSCs for SOM^{Cre}-negative neurons was 7.0 ± 0.2 ms, which was delayed in comparison with the short latency of Aβ-eEPSCs (3.2 ± 0.5 ms, two-tailed Student's unpaired test, p < 0.001),

but well preceded the onset of the first Aβ-eAP under the disinhibition condition (48.3 ± 10.9 ms, two-tailed Student's unpaired test, $p < 0.001$) (Figure 2C). We refer to these latencies as t_{IPSC}, t_{EPSC}, and t_{AP}, respectively in Figure 2C.

We then asked why SOM^{Cre}-negative neurons in $_{v}II_{i}$-$_{d}III$ require such long latencies to fire APs under disinhibition conditions. Following glutamatergic excitatory synaptic transmission, activation of different glutamate receptors has distinct kinetics: AMPARs (α-amino-3-hydroxy-5-methyl-4-isoxazolepropionic acid receptors), a class of non-NMDARs, show rapid ligand-gated activation, whereas NMDARs (N-methyl-D-aspartate receptors) are more than ten-fold slower (Edmonds et al., 1995). To assess the roles of NMDARs in driving slow-onset AP firing, we included MK-801 (2 mM) in the recording electrode to block postsynaptic NMDARs (Huettner and Bean, 1988) in individual recorded neurons. MK-801 indeed caused a reduction of SOM^{Cre}-negative neurons with Aβ-eAPs, from 100% (14 of 14) without MK-801 to 39% (7 of 18) with MK-801 (Chi-square test, $p < 0.01$). Thus, for a majority of these neurons (61%), Aβ-evoked AP firing under the disinhibition condition requires NMDAR currents. This percentage (61%) is likely underestimated because the remaining 39% may receive convergent polysynaptic inputs not blocked by MK-801 when it was only applied to the recorded neurons (Figure 2B).

In summary, these results reveal a time control mechanism to achieve gate control. First, fast non-NMDAR-evoked EPSPs are subthreshold, and Aβ-evoked AP firing requires activation of slow-onset NMDARs. Secondly, IPSCs arrive before, and act to suppress, NMDAR-dependent AP firing. In other words, it is the dependency on slow-onset and long-lasting NMDAR currents for AP firing that creates a time window for feedforward inhibition to operate.

Gate opening mechanisms by capsaicin at the II-III border

We next asked how hindpaw capsaicin injection allowed SOM^{Cre}-negative neurons in $_{v}II_{i}$-$_{d}III$ to overcome gate control and produce Aβ-eAPs. We first examined the timing of firing. Following capsaicin treatment, the latency for SOM^{Cre}-negative neurons in $_{v}II_{i}$-$_{d}III$ to fire AP (t_{AP}) is around 7.7 ± 0.9 ms (Figure 3B and 3C), which is much shorter than the latency observed under pure disinhibition conditions without capsaicin treatment (see Figure 2C; 48.3 ± 10.9 ms, two-tailed Student's unpaired test, $p < 0.001$). Inclusion of the NMDAR blocker MK-801 (2 mM) in the recording electrode did not change the percentage of neurons producing Aβ-eAPs: 59% (13 of 22) with MK-801 versus 56% (19 of 34) without MK-801 (Chi-square test, $p = 0.813$) (Figure 3E and 3F), indicating that Aβ stimulation-induced non-NMDAR inputs became suprathreshold after capsaicin injection.

In the gate control theory, nociceptor inputs are postulated to reduce inhibitory neuron activity (Figure 1A). We therefore examined how Aβ-evoked IPSCs were affected. Surprisingly, we found that following capsaicin injection 71% (12 of 17) of SOM^{Cre}-negative neurons in $_{v}II_{i}$-$_{d}III$ showed detectable Aβ-eIPSCs, a percentage much higher than that in naive mice (38%, 11 of 29, Chi-square test, $p < 0.05$) (Figure 3D). Consistently, $Pdyn^{Cre}$-derived inhibitory neurons in $_{v}II_{i}$-$_{d}III$, which are necessary for gating Aβ inputs (Duan et al., 2014), were sensitized by capsaicin (Figure S3). Thus, at least a subset of SOM^{Cre}-negative neurons (71% - 38% = 33%) gained de novo Aβ-eIPSCs following

capsaicin treatment (Figure 3D), rather than a loss according to the original gate control theory (Figure 1A). We then further compared the mean latencies of Aβ-eIPSCs (t_{IPSCs}) under naïve conditions versus Aβ-eAPs (t_{APs}) after capsaicin treatment, and found that for neurons with AP firing, 74% (14 of 19) fired before the mean latency of IPSCs (7.4 ms) (Figure 3C), indicating that by the time inhibitory inputs arrived, non-NMDAR currents had already caused AP firing, thereby bypassing the gate control.

What roles did Aβ-evoked inhibitory inputs to SOM^{Cre}-negative neurons play after capsaicin treatment? As described in Figure 1F, following capsaicin treatment, 74% (14 of 19) of SOM^{Cre}-negative neurons with Aβ-eAPs in $_{v}II_{i}$-$_{d}III$ receive monosynaptic Aβ inputs, and among these neurons, 71% (10 of 14) can only fire one spike (Figure 1F). We then found that for slices from mice with capsaicin treatment, bath application of bicuculline and strychnine caused prolonged firing in SOM^{Cre}-negative neurons, with the number of Aβ-eAPs increasing to 10.1 ± 1.9, in comparison with 1.6 ± 0.3 without bicuculline and strychnine (two-tailed Student's unpaired test, $p < 0.001$) (Figure 3F). Including MK-801 in the recording electrode to block NMDARs caused a reduction in AP numbers, from 10.1 ± 1.9 to 4.7 ± 1.5 (two-tailed Student's unpaired test, $p < 0.05$) (Figure 3F). Thus, following capsaicin treatment, feedforward inhibition via activation of bicuculline/strychnine-sensitive $GABA_A$ and glycine receptors switches to control firing duration, partly by blocking MK-801-senstive NMDARs.

Together, the above recordings in the lamina II and III border area show that capsaicin-mediated nociceptor inputs can overcome gate control by sensitizing non-NMDAR-mediated excitatory inputs, to a degree that APs fire before evoked IPSCs arrive, in striking contrast to NMDAR-dependent slow firing under pure disinhibition conditions with bicuculline and strychnine (summarized in Figure 3G). Against the prediction of the original gate control theory, capsaicin sensitized inhibitory neurons and the expanded Aβ-eIPSCs instead act to control AP firing duration (Figure 3G).

Gating mechanism in I-II_o: the roles of electric filtering by potassium channels

We next investigated gate control mechanisms for SOM^{Cre}-negative neurons located in I-II_o. By performing the same set of recordings described in Figure 2, we found that 53% (21/40) and 43% (10/23) of these neurons showed Aβ eEPSCs and eIPSCs, respectively (Figures 1E and S4B), but only 10% (4/40) produced Aβ eAPs (Figure 1E). Most neurons with eIPSCs (90%: 9/10) concurrently contain eEPSCs, and they used the same time control mechanisms to achieve gate control: Aβ-evoked non-NMDAR inputs are subthreshold, and Aβ-eIPSCs prevent NMDAR-dependent AP firing (Figure S4B and S4C).

We next investigated the mechanistic basis underlying the subthreshold nature of fast non-NMDAR-mediated inputs, and revealed a crucial role of potassium channel activity, including I_A mediated by A-type voltage-dependent potassium channels that display characteristic fast activation and fast inactivation kinetics (Hu et al., 2006). The existence of strong I_A in SOM^{Cre}-negative neurons within I-II_o was first suggested from the delayed firing pattern following 150 pA current injection in 46% (18/39) of these neurons (with firing latencies at 223.6 ± 35.8 ms) (Figure 4C). Delayed firing can result from the activity of subthreshold potassium channels, such as I_A (Shibata et al., 2000). To record and isolate

I_A, we used a two-step voltage protocol (Hu et al., 2006; Hu et al., 2003) (Figure 4B). To test the role of I_A and other potassium channel activity, we included 4-AP (2 mM) in the recording electrode, which caused a marked reduction of I_A in individually recorded neurons (control: median, 808 pA; Q1–Q3, 350–1576 pA; 4-AP: median, 157 pA; Q1–Q3, 52–468 pA, Mann-Whitney Rank Sum Test, $p < 0.001$) (Figure 4B). 4-AP also caused a trend of reduction in persistent potassium channel activity (I_D), although the reduction does not reach significance (control: median, 1361 pA; Q1–Q3, 813–3518 pA; 4-AP: median, 888; Q1–Q3, 350–2203 pA, Mann-Whitney Rank Sum Test, $p = 0.191$) (Figure 4B). Following this blockage of potassium channel activity, 150 pA current injection drove most SOM^{cre}-negative neurons (91%, 21/23) to fire with short latencies (24.9 ± 2.9 ms); in other words, those 46% SOM^{cre}-negative neurons with long delayed firing under normal conditions were converted to fire with fast kinetics following potassium channel blockage (Figure 4C).

We next examined how potassium channel blockage affected Aβ inputs to SOM^{Cre}-negative neurons in I-II_o. Strikingly, including 4-AP in the recording electrode led to Aβ-eEPSPs in virtually all neurons (96%, 24/25), increased from 53% (21 of 40) without 4-AP (Chi-square test, $p < 0.001$) (Figure 4D). Furthermore, 69% (18 of 26) of SOM^{Cre}-negative neurons in I-II_o started to produce Aβ-eAPs, a marked increase from 10% (4 of 40) without 4-AP (Chi-square test, $p < 0.001$) (Figure 4D). Thus, potassium channel blockage in individually recorded neurons can bypass gate control, allowing Aβ stimulation to fire APs in a majority of SOM^{Cre}-negative neurons in I-II_o. The latency of Aβ-eAPs with 4-AP treatment (11.3 ± 1.3 ms) was much shorter than that under the pure disinhibition condition with the presence of bicuculline and strychnine (60.3 ± 7.3 ms, two-tailed Student's unpaired test, $p < 0.001$) (Figure 4D). For 4-AP-sensitized neurons with Aβ-eAPs, nearly 40% (7 of 18) fired before the mean latency of Aβ-eIPSCs detected under normal conditions (8.5 ms) (Figure 4D). Furthermore, inclusion of both 4-AP and MK-801 in the recording electrode still drove 48% (12/25) of SOM^{Cre}-negative neurons to produce Aβ-eAPs (Figure 4D). In other words, nearly 70% of neurons sensitized by 4-AP bypass NMDAR dependency to fire APs (48% with MK-801 versus 69% without MK-801; 48/69 = 70%).

These recordings suggest that 4-AP-sensitive potassium channel activity can either completely filter away Aβ inputs for those neurons that normally do not produce Aβ-eEPSPs (Figure 4F, left), or convert otherwise "suprathreshold" non-NMDAR inputs to become subthreshold, such that feedforward inhibition can now gain time to prevent NMDAR-dependent slow-onset AP firing (Figure 4F, right). This potassium channel-mediated control mechanism was unique for neurons in I-II_o, since 4-AP treatment was insufficient to cause Aβ-eAPs in SOM^{Cre}-negative neurons within $_vII_i$-$_dIII$ (10%, 3/29 without 4-AP versus 7%, 1/15 with 4-AP; Chi-square test, $p = 1.000$) (Figure 4E).

We subsequently found that the masked Aβ inputs to I-II_o neurons uncovered by 4-AP were lost in SOM^{Lbx1}-ablated mice (Figure S5). To explain such loss, Aβ inputs were likely relayed indirectly via type 1 SOM^{Cre}-derived interneurons that produce Aβ-eAPs under normal conditions (Duan et al., 2014), since type 2 and type 3 SOM^{Cre}-derived neurons would still be gated by feedforward inhibition (Duan et al., 2014) when 4-AP was delivered to individual SOM^{Cre}-negative neurons in I-II_o via the recording electrode. Type 1 SOM^{Cre}-derived neurons are located in $_vII_i$-$_dIII$ and possibly in more ventral regions as well (Duan et

al., 2014), and accordingly, low threshold Aβ mechanoreceptors that innervate laminae III-V could be the source for silent Aβ inputs (summarized in Figure 4F). High threshold Aβ mechanical nociceptors, which innervate throughout the dorsal horn (Boada and Woodbury, 2008), could be another source, but their involvement would make it difficult to explain the reliance on type 1 SOM^{Cre}-derived neurons located in $_{v}II_{i}$-$_{d}III$ and the lamina III.

Gate opening by capsaicin in I-II_o: central sensitization partly via I_A reduction

We next asked how capsaicin injection caused SOM^{Cre}-negative neurons in I-II_o to fire APs in response to Aβ stimulation. As the case in $_{v}II_{i}$-$_{d}III$, several lines of studies show that this gate opening is not due to inactivation of inhibitory neurons, against a key tenet of the original gate control theory (Figure 1A). First, capsaicin injection led to an increase in Aβ-eAPs in $Pdyn^{Cre}$-derived inhibitory neurons in I-II_o, from 56% (25 of 45) in control mice to 83% (15 of 18, Chi-square test, $p < 0.05$) in capsaicin-injected mice (Figure S6A). Such sensitization was also observed when the whole spinal inhibitory neuronal population marked by $VGAT^{Cre}$ was analyzed (Figure S1). Accordingly, there is a trend that more SOM^{Cre}-negative neurons received Aβ-evoked IPSCs, from 43% (10/23) in control mice to 67% (12/18) in capsaicin-injected mice (Figure S6B). Second, current clamp recordings showed that the latencies of Aβ-eAPs firing in SOM^{Cre}-negative neurons (t_{AP}) are around 8.4 ± 0.8 ms (Figure 5B), which is much shorter than that caused by disinhibition with the presence of bicuculline and strychnine (60.3 ± 7.3 ms, two-tailed Student's unpaired test, $p < 0.001$). Furthermore, 71% (15 of 21) of SOM^{Cre}-negative neurons fired before the mean arrival latency of IPSCs (8.5 ms) (Figure 5B), thereby bypassing feedforward inhibition. This rapid firing suggests that Aβ evoked non-NMDAR inputs most likely become suprathreshold following capsaicin treatment, bypassing NMDAR dependency. Indeed, when we included MK-801 (2 mM) in the recording electrode to block postsynaptic NMDARs, the percentage of neurons with Aβ-eAPs was not changed dramatically (50%, 10 of 20 with MK-801 versus 67%, 22 of 33 without MK-801, Chi-square test, $p = 0.229$) (Figure 5B).

We next explored what capsaicin-induced changes drove fast Aβ-eAPs. We first found that the resting membrane potentials (RMPs) of SOM^{Cre}-negative neurons in I/II_o were slightly depolarized, from −74.4 ± 0.9 mV in control mice to −71.3 ± 1.2 mV following capsaicin injection (two-tailed Student's unpaired test, $p < 0.05$) (Figure S7A), suggesting a potential increase in sodium channel activity and/or a decrease in potassium channel activity that controls resting membrane potentials; however, this small degree of depolarization alone appears insufficient to cause Aβ-eAPs (Figure S7B). We then found that capsaicin treatment caused a marked reduction in I_A currents in SOM^{Cre}-negative neurons (control: median, 538 pA; Q1–Q3: 297–1406 pA; capsaicin treatment: median, 298 pA; Q1–Q3, 150–551 pA; Mann-Whitney Rank Sum Test, $p < 0.05$) (Figure 5C). Since a blockage of subthreshold potassium channel activity is sufficient to generate Aβ-eAPs, such I_A reduction should contribute to capsaicin-induced gate opening.

In dorsal horn neurons, I_A is mainly contributed by the Kv4.2 potassium channel (Hu et al., 2006) and Kv4.2 activity can be inactivated following phosphorylation by the extracellular signal-regulated kinases (ERKs) (Adams et al., 2000). Hindpaw capsaicin injection is known

to induce phosphorylation and subsequent activation of ERK in superficial dorsal horn neurons, and this activation is dependent on the upstream kinase MEK (Jin et al., 2003). We confirmed that intrathecal injection of the MEK kinase inhibitor PD98059 blocked ERK activation (Figure S8A). With this blockage, capsaicin injection failed to cause i) I_A current reduction (Figure 5C), ii) Aβ-evoked AP firing (Figure 5D) in SOM^{Cre}-negative neurons within I-II_o, and iii) manifestation of punctate and dynamic forms of mechanical hypersensitivity (Figure S8B). Thus, strong nociceptor inputs evoked by hindpaw capsaicin injection open the gate, partly by reducing subthreshold potassium channel activity via the activation of the MEK-ERK signaling.

Constitutive activity of $Pdyn^{Cre}$-derived inhibitory neurons controls the I_A size

We next asked how I_A currents are established in SOM^{Cre}-negative neurons in I-II_o. We reported previously that $Pdyn^{Cre}$-derived inhibitory neurons are required to gate Aβ inputs to neurons in I-II_o (Duan et al., 2014). In mice with selective ablation of spinal inhibitory neurons marked by coexpression of $Pdyn^{Cre}$ and $Lbx1^{Flpo}$, referred to as $Pdyn^{Lbx1}$-ablated mice, 76% of neurons in I-II_o generated Aβ eAPs, in comparison with 7% in control mice, indicating the loss of gate control (Duan et al., 2014). $Pdyn^{Cre}$-derived neurons can be sub-divided according to persistent versus transient $Pdyn^{Cre}$ expression (Duan et al., 2014). Chemical genetic silencing of spinal neurons with persistent $Pdyn^{Cre}$ expression led to partial gate opening and manifestation of both punctate and dynamic mechanical hypersensitivity (Figure S9A–D). Thus, adult $Pdyn^{Cre+}$ spinal neurons are required to gate mechanical sensitivity, besides a role of these neurons in gating itch (Huang et al., 2018; Kardon et al., 2014; see also the legend of Figure S9C). For this study, we only focused on how $Pdyn^{Lbx1}$ neurons gate Aβ inputs to neurons in I-II_o.

We first revisited firing latencies. To our great surprise, 54% (13/24) of I-II_o neurons fired APs within 10 ms in $Pdyn^{Lbx1}$-ablated mice (Figure 6A), in contrast to 60 ms on average under disinhibition with bicuculline and strychnine (Figure 5A). This rapid firing is nonetheless comparable to the short firing latencies caused by capsaicin injection or potassium channel blockage by 4-AP. We next postulated that $Pdyn^{Cre}$-derived inhibitory neurons might have a constitutive role, releasing mediators that establish proper levels of subthreshold potassium activity. Indeed, 31% (7 of 23) of $Pdyn^{Cre}$-$tdTomato^{+}$ neurons in I-II_o fired spontaneously (Figure 6B). We then measured and found that in $Pdyn^{Lbx1}$-ablated mice, the I_A sizes in I-II_o neurons were reduced significantly in comparison with control littermates (control: median, 533 pA; Q1–Q3: 302–1532 pA; Ablated mice: median, 288 pA; Q1–Q3, 86–516 pA; Mann-Whitney Rank Sum Test, $p < 0.001$) (Figure 6C). No significant changes in resting membrane potentials were detected (control: −72.6 ± 2.0 mV; ablated mice: −71.6 ± 1.0 mV, two-tailed Student's unpaired test, $p = 0.708$). This marked I_A reduction is analogous to that caused by hindpaw capsaicin injection in $Pdyn^{Cre}$-negative neurons (Figure S10), which may partly explain the rapid AP firing following Aβ stimulation in both $Pdyn^{Lbx1}$-ablated mice and capsaicin-treated wild type mice.

DISCUSSION

Timing mechanisms underlying gate control by feedforward inhibition

Most neurons in the superficial dorsal horn receive direct or indirect Aβ afferent inputs without AP outputs due to feedforward inhibition (Duan et al., 2018; Takazawa and MacDermott, 2010), such that innocuous mechanical stimuli do not evoke pain under normal conditions. For those with direct Aβ inputs, such as SOM^{Cre}-negative neurons in $_{v}II_{i}$-$_{d}III$, they face a timing question as to how monosynaptic excitatory inputs can be gated by di-synaptic inhibitory inputs. Our results indicate that the amplitudes and kinetics of different glutamate receptors are part of the solution. Non-NMDARs, such as AMPARs, have rapid kinetics of activation and decay, with currents rising in less than 1 ms and decaying with a time constant between 0.2 and 8 ms (Edmonds et al., 1995). In contrast, activation of NMDARs requires 10–20 ms to reach the peak, and then decays over hundreds of ms (Edmonds et al., 1995). Here we found that following dorsal root stimulation at ~8 mm away from the dorsal entry zone (Cheng et al., 2017), the mean latency of Aβ-evoked IPSCs in SOM^{Cre}-negative neurons in $_{v}II_{i}$-$_{d}III$ (recorded from the soma) is around 7.4 ms, which is 3–4 ms after the arrival of Aβ-evoked non-NMDAR-dependent EPSCs, but before NMDAR currents reach the peak. We then find that under disinhibition conditions by blocking $GABA_A$ and glycine receptors, Aβ-evoked non-NMDAR-dependent EPSPs are subthreshold, requiring MK-801-sensitive NMDAR currents to drive AP firing; as such, average AP firing latencies are 48 ms and 60 ms for neurons in $_{v}II_{i}$-$_{d}III$ and I-II_{o}, respectively (Figure 2 and Figure 4). In other words, Aβ-eIPSCs arrive long before eEPSPs reach the firing threshold. We then found that for neurons in I-II_{o}, potassium channel activities along the dendrites to the soma either completely filter away Aβ inputs (see below for more detailed discussion), or transform Aβ-evoked fast non-NMDAR-dependent inputs to become subthreshold, thereby creating a permissive condition for feedforward inhibition to operate. Thus, distinct glutamate receptor kinetics plus electric filtering by potassium channels jointly solve a timing problem, allowing delayed arrival of inhibitory inputs to achieve the gate control.

Electric filtering by potassium channels creates “silent” Aβ inputs

For ~50% I-II_{o} neurons that normally do not show Aβ-eEPSPs (and Aβ-eIPSCs), a blockage of potassium channels activity by 4-AP reveals massive “silent” Aβ inputs to these neurons. These “silent” inputs are likely relayed via un-gated type 1 SOM neurons (Figure 4F and Figure S5), distinct from polysynaptic Aβ inputs gated via feedforward inhibition operating in $_{v}II_{i}$-$_{d}III$ (Duan et al., 2018). Besides the gate control theory of pain, Wall and others introduced the concept of effective versus ineffective synapses (Gobel and Dubner, 1969; Merrill and Wall, 1972). This concept is built upon observations from extracellular recordings, showing that the distal dendrites of a spinal neuron in lamina IV can receive “ineffective” synaptic inputs from afferents that do not project to the “effective” receptive field, and such inputs do not produce firing unless synchronized electric stimulation was used (Merrill and Wall, 1972). Other studies in 1990s led to the discovery of “silent synapses” caused by a lack of AMPARs in the postsynaptic membrane (Kerchner and Nicoll, 2008), which are particularly abundant in the developing brain and spinal cord (Bardoni et al., 1998; Bloodgood and Sabatini, 2008; Li and Zhuo, 1998; Petralia et al.,

1999). The unmasking of "silent" fast-onset Aβ inputs to spinal I-II_o neurons following blockage of potassium channels in individually recorded neurons (Figure 4), however, argues against a lack of AMPARs in the postsynaptic membrane.

Where do potassium channels operate to filter away Aβ inputs? Interneurons in I-II_o include vertical cells or other cells with dendrites reaching $_vII_i$-$_dIII$ or more ventral laminae, which could receive more direct Aβ inputs (Cordero-Erausquin et al., 2009; Duan et al., 2014; Gobel, 1978). Consistently, Golgi staining revealed dense spines in the distal dendrites of these cells (Gobel, 1978), and such spines are the sites for excitatory glutamatergic synaptic transmission (Nimchinsky et al., 2002), though recent studies show that inhibitory synaptic transmission can concurrently occur in spines (Chiu et al., 2013). To some degree these vertical cells mimic pyramidal neurons with elaborate dendritic trees in the cortex and hippocampus. For those pyramidal neurons, synaptic inputs to distal dendrites from other cortical areas are also ineffective due to strong electric filtering mediated by potassium channels, particularly the I_A currents (Hoffman et al., 1997; Harnett et al., 2013; Major et al., 2013; Stuart and Spruston, 2015). In superficial dorsal horn neurons, Kv4.2 contributes to I_A currents (Hu et al., 2006) and is enriched in the dendrites (Huang et al., 2005; Trimmer, 2015). Mice with deficiency of Kv4.2 showed mechanical hypersensitivity (Hu et al., 2006). Thus, Kv4.2 is a candidate acting to neutralize Aβ-evoked EPSPs along the distal dendrite to the soma. Amazingly, back to early 1970s, Merrill and Wall already postulated an electric constriction at the base of spines and/or in distal dendrites to explain ineffective-silent synaptic inputs (Merrill and Wall, 1972)! It should be noted that for vertical cells receiving silent Aβ inputs in distal dendrites, the cell bodies are located in II_o and their proximal dendrites receive inputs from C/Aδ nociceptors (Braz et al., 2014). Due to a lack of detectable Aβ-eIPSCs in these neurons, we might envision a scenario allowing positive temporal integration of inputs from these fibers with distinct conduction velocities. For example, in response to noxious stimuli, these cells would first receive fast-conducting "ineffective" Aβ inputs, leading to activation and then inactivation of I_A currents, and this I_A inactivation might in turn influence the outputs when slow-conducting C/Aδ nociceptor inputs arrive. Future studies will be warranted to test this hypothesis.

Constitutive activity of spinal inhibitory neurons sets up gate control

Four groups of genetically labeled spinal inhibitory neurons participate in gating Aβ inputs to spinal pain transmission T neurons. $Pdyn^{Cre}$-derived inhibitory neurons are mainly GABAergic and enriched in superficial laminae (Duan et al., 2014), whereas those marked by the expression of $Parvalbumin^{Cre}$, $GlyT2^{Cre}$, and Ret^{Cre} are enriched in deep dorsal horn laminae and release glycine and/or GABA (Cui et al., 2016; Foster et al., 2015; Lu et al., 2013; Petitjean et al., 2015; Takazawa et al., 2017). Here, our timing analyses reveal an unsuspected insight: the constitutive activity from $Pdyn^{Cre}$-derived inhibitory neurons is required to set up a permissive condition to achieve gate control. In $Pdyn^{Lbx1}$-ablated mice, a majority of I-II_o neurons fire within 10 ms in response to Aβ stimulation (Figure 6). In contrast, upon blockage of bicuculline-sensitive $GABA_A$ and strychnine-sensitive glycine receptors, the mean latency of Aβ-evoked AP firing is around 60 ms (Figure 6). Since bicuculline plus strychnine can block most IPSCs in dorsal horn excitatory neurons (Takazawa et al., 2017), we are not aware of other evoked feedforward inhibition

mechanisms that could operate within 10 ms. For example, activation of G-protein coupled inhibitory receptors, such as the $GABA_B$ receptor and opioid peptide receptors, needs at least 40 ms (Vilardaga et al., 2003). This paradox is solved by the findings that $Pdyn^{Cre}$-derived neurons fire spontaneously, and ablation of these inhibitory neurons leads to a marked reduction in I_A sizes for neurons in I-II_o (Figure 6). Thus, fast Aβ-evoked AP firing in $Pdyn^{Lbx1}$-ablated mice apparently mimics the situation caused by the blockage of potassium channels in naïve mice. The mediators released from $Pdyn^{Cre}$-derived neurons remain to be determined. One candidate is the dynorphin peptide itself. Bath application of nor-BNI, an antagonist of the dynorphin receptor KOR (Portoghese et al., 1987; Kardon et al., 2014), partially opened the gate (Figure S11). Behaviorally, intrathecal injection of this drug resulted in both punctate and dynamic mechanical hypersensitivity (Figure S11), not just itch sensitization (Kardon et al., 2014), consistent with the gating of both mechanical pain and itch by potentially different subsets of $Pdyn^{Cre}$-derived inhibitory neurons (Duan et al., 2014; Huang et al., 2018; Kardon et al., 2014).

Thus, spinal inhibitory neurons have two roles in setting up gate control. The constitutive activity of $Pdyn^{Cre}$-derived inhibitory neurons establishes proper levels of subthreshold potassium channel activity, whose electric filtering creates a permissive condition to achieve gate control by preventing fast-onset non-NMDAR-evoked inputs from causing firing. Evoked activity of $Pdyn^{Cre}$-derived and $Pdyn^{Cre}$-negative inhibitory neurons then carries out the actual feedforward inhibition to prevent NMDAR-dependent firing.

How do strong nociceptor inputs open the gate?

A key tenet of the original gate control theory of pain is that strong C/Aδ fiber inputs to the spinal cord open the gate by inactivating the inhibitory neurons (Melzack and Wall, 1965) (Figure 1A). We, however, found that capsaicin-activated nociceptor inputs in fact sensitize both $Pdyn^{Cre}$-derived and $VGAT^{Cre}$-derived inhibitory neurons (Figures S1 and S6), leading to a net increase in the percentage of SOM^{Cre}-negative neurons in I-II_o that produce Aβ-evoked IPSCs (Figure S6), even though IPSC reduction may occur in some dorsal horn neurons (Lin et al., 1996). Rather, capsaicin treatment allows Aβ-evoked non-NMDAR-mediated inputs to cause AP firing before feedforward inhibition starts to operate, and the sensitized Aβ-evoked inhibitory inputs switch to control firing duration, rather than firing prevention. This is achieved via sensitization of spinal transmission T neurons through multiple mechanisms, including I_A reduction (Figure 5), depolarization of resting membrane potentials (RMPs, Figure S7), and increased AMPAR trafficking (Kopach et al., 2011; Lee et al., 2012; Tao, 2012). The modest changes in RMPs (from −74 to −71 mV) unlikely cause activation and then inactivation of A type potassium channels, since the half-maximal activation and inactivation potentials for I_A are around −6 mV and –51 mV, respectively (Hu et al, 2003). Kv4.2 can be inactivated via ERK-mediated phosphorylation (Adams et al., 2000; Hu et al., 2007), and strong nociceptor inputs, such as those evoked by capsaicin injection, can induce pERK in most superficial dorsal horn (Ji et al., 1999) (Figure S8), which could in principle lead to I_A reduction. Thus, I_A reduction following strong nociceptor inputs essentially produces a novel form of disinhibition, by overcoming electric filtering that is permissive for gate control and whose capacity is constitutively established by $Pdyn^{Cre}$-derived inhibitory neurons.

This sensitization-dominant gate opening mechanism caused by acute intense nociceptor inputs, which could occur during any traumatic tissue injury, is therefore different from the loss of Aβ-eIPSCs following nerve injury or chronic inflammation (Bonin and De Koninck, 2013; Latremoliere and Woolf, 2009; Lu et al., 2013; Petitjean et al., 2015; Prescott, 2015; Takasawa et al., 2017; Zeilhofer et al., 2012). Interestingly, VGLUT3^{Cre}-derived spinal neurons are required to transmit brush-evoked dynamic allodynia induced by inflammation or nerve injury (Cheng et al., 2017), but not the one induced by capsaicin (Figure S2). The existence of distinct gate opening mechanisms and underlying spinal substrates suggests the necessity of developing distinct strategies for treating different forms of pathological pain.

STAR★METHODS

KEY RESOURCES TABLE

REAGENT or RESOURCE	SOURCE	IDENTIFIER
Antibodies		
Rabbit Anti-c-Fos Antibody	Millipore	Cat# ABE457 RRID: AB_2631318
Rabbit Anti-pERK Antibody	Cell signaling technology	Cat# 4370S RRID: AB_2315112
Rabbit Anti-GFP	ThermoFisher Scientific	Cat# A-11122 RRID: AB_221569
Goat Anti-Rabbit IgG, Alexa Fluor 488	Invitrogen	Cat# A11034 RRID: AB_2576217
Chemicals		
Capsaicin	Sigma	Cat# M2028
1(S),9(R)-(−)-Bicuculline methiodide	Sigma	Cat# 14343
Strychinine hydrochloride	Sigma	Cat# S8753
QX-314	Sigma	Cat# L5783
(+)-MK-801 hydrogen maleate	Sigma	Cat# M107
4-Aminopyridine	Sigma	Cat# 275875
nor-NBI	Sigma	Cat# N1771
PD98059	Sigma	Cat# P215
SALB	Sigma	Cat# 75250
Diphtheria toxin	Sigma	Cat# D0564
Tetrodotoxin citrate	Abcam Biochemicals	Cat# ab120055
Plasmid pAAV-hSyn-dF-HA-KORD-IRES mCitrine	Addgene	Cat# 65417
Expenmental Models:Strains		
Mouse: STOCK *Sst<tm2.1(cre)Zjh>J (Somatostatin-IRES-Cre)*	Jackson Laboratory	RRID: IMSR_JAX:013044
Mouse: B6; 129S-Pdyntm1.1(cre)Mjkr/LowlJ (*Prepmdynorphin-IRES-Cre*)	Jackson Laboratory	RRID: IMSR_JAX:027958
Mouse: B6;129S-VGLUT3<tm1Lowl> *(Vglut3-Cre)*	Generated by Lowel Lab	Cheng et al., 2017
Mouse: B6;129S6-Gt(ROSA)26Sortm14(CAG-tdTomato)Hze/J (*ROSA26CAG-loxP-STOP-loxP-tdTomato reporter)*	Jackson Laboratory	RRID: IMSR_JAX:007908
Mouse: B6;129S-Lbx1<tm1(flpo)Gou> *(Lbx1-Flpo)*	Generated by Goulding Lab	Bourane et al., 2015, Science
Mouse: B6.129-Tau<tm1(LSL.FSF.DTR)Gou> (*Tau-loxP-STOP-loxP-FRT-STOP-FRT-DTR)*	Generated by Goulding Lab	Bourane et al., 2015, Cell
Mouse: STOCK Slc32a1tm2(cre)Lowl/J (*Vgat-IRES-Cre*)	Jackson Laboratory	RRID: IMSR_JAX:016962
Software		
Excel	Microsoft	N/A
pClamp 10.0	Molecular Devices	RRID:SCR_011323
Prism 7	GraphPad	RRID: SCR_002798

CONTACT FOR REAGENT AND RESOURCE SHARING

Further information and requests for resources, reagents and data should be directed to and will be fulfilled by the Lead Contact, Qiufu Ma (Qiufu_Ma@dfci.harvard.edu).

EXPERIMENTAL MODEL AND SUBJECT DETAILS

Experimental Animals—All animal experiments, including behavioral tests, were performed with protocols approved by the Institutional Animal Care and Use Committee at Dana-Farber Cancer Institute. Mice were housed at room temperature with a 12-h/12-h light/dark cycle and ad libitum access to standard lab mouse pellet food and water. The genetically modified mice used in this study, including *Somatostatin-IRES-Cre* (*SOM*^{Cre}), *Preprodynorphin-IRES-Cre* (*Pdyn*^{Cre}), *Vglut3*^{Cre}, the ai14 *ROSA26CAG-loxP-STOP-loxP-tdTomato* reporter, *Lbx1*^{Flpo}, *Tau-loxP-STOP-loxP-FRT-STOP-FRT-DTR*, and *Slc32a1-IRES-Cre* (*VGAT*^{Cre}) had been reported previously (Bourane et al., 2015a; Bourane et al., 2015b; Cheng et al., 2017; Krashes et al., 2014; Madisen et al., 2010; Taniguchi et al., 2011; Vong et al., 2011). To ablate DTR-expressing neurons for behavioral studies, mice of 6–10 weeks old were intraperitoneally injected with the diphtheria toxin (DTX, 50 μg/kg; Sigma-Aldrich, USA) at day 1 and then again at day 4. Behavioral experiments were performed 4 weeks after DTX injection. To ablate DTR-expressing neurons for electrophysiological recording, mice (P18–P21) were intraperitoneally injected with the diphtheria toxin (DTX, 50 μg /kg) at day 1 and then again at day 4. Recordings were performed 7–12 days after the first DTX injection (P26–P30). Both males and females were used. Animals were assigned to treatment groups in a blinded fashion, and pain responses were measured in a blinded manner.

METHOD DETAILS

Behavioral Testing—All animals were acclimatized to the behavioral testing apparatus for 30 min/d for 3 consecutive days before testing. After habituation, baseline measurements were recorded on two consecutive days prior to different treatment. To test capsaicin-induced mechanical hypersensitivity, 0.3 μg/10 μl capsaicin (in saline solution containing 7% Tween 80, 20% ethanol) was injected intradermally into the plantar region of the left hindpaw. After capsaicin injection, behavioral tests were performed at defined intervals. Acute licking duration was measured at first 5 min after capsaicin injection. Both punctate and dynamic forms of mechanical hypersensitivity were measured before capsaicin injection, and then at 15, 30, 60, 90 and 120 min after capsaicin injection. All data points were included for subsequent statistical analyses. Control animals were littermates of SOM^{Lbx1}-ablated mice or VGLUT3^{Lbx1}-ablated mice lacking DTR expression but receiving the same DTX injection. The following pairs of mice were also subjected to behavioral analyses, including i) Pdyn^{Cre}-KORD mice and their control mice treated with SALB, ii) wild type mice with or without hindpaw capsaicin injection, iii) capsaicin-injected wild type mice treated with or without PD98059, or iv) wild type mice treated with or without nor-BNI (for detailed description of these treatments, see below). Dynamic mechanical hypersensitivity was measured by light stroking (velocity: ~2 cm/s; from heel to toe) across the plantar area of the injected hind paw using a trimmed paintbrush (Size 2, Model 8795, Raphael Kaerell Co.), as described previously (Cheng et al., 2017). The typical response of

naive mice is a very fast movement, lifting the stimulated paw for less than 1 s (score 0). After capsaicin treatment, several pain-suggestive responses evoked by brushing can be observed, such as sustained lifting (more than 2 s) of the stimulated paw toward the body or a single gentle flinching of the stimulated paw (score 1); one strong lateral paw lift, above the level of the body or a startle-like jump (score 2); and multiple flinching responses or licking of the affected paw (score 3). We repeated the stimulation three times at ~10 s intervals and obtained an average score for each mouse, as described previously (Cheng et al., 2017). Punctate mechanical hypersensitivity was measured by stimulating the heal of the injected hindpaw with von Frey filaments, and the thresholds causing withdrawal responses were determined using Dixon's up–down method (Chaplan et al., 1994).

To test involvement of SOM-linage neurons or VGLUT3-linage neurons in capsaicin-induced acute licking responses and/or mechanical hypersensitivity, littermates of SOM^{Lbx1}-ablated mice or $VGLUT3^{Lbx1}$-ablated mice lacking DTR expression but receiving the same DTX (50 μg/kg in 200 μl PBS for 30g mice) injection were used as control. One month after first DTX injection, hindpaw injection of capsaicin (0.3 μg/10 μl) was performed, and the licking responses were recorded and analyzed in a 15-min period following injection. Punctate and dynamic forms of hypersensitivity were measured at 15, 30, 60, 90 and 120 min after capsaicin injection. To test the involvement of the ERK signaling pathway in capsaicin-induced mechanical hypersensitivity, the MEK inhibitor PD98059 (Sigma, 0.5 μg in 10 μl 10% DMSO) or vehicle (10 μl 10% DMSO) was intrathecally injected and then flushed with 10 μl of saline at 30 min before capsaicin injection. Both punctate and dynamic forms of mechanical hypersensitivity were measured at 15, 30, 60, 90 and 120 min after capsaicin injection. To test acute silencing of $Pdyn^{Cre}$-expressing neurons on mechanical hypersensitivity, SALB (60 μl, 10mg/kg, dissolved in DMSO) were subcutaneously injected at upper back area in control WT mice and in $Pdyn^{Cre}$-KORD mice 3 weeks after intraspinal virus injection. The punctate and dynamic forms of mechanical hypersensitivity were then measured at 30 min and 60 min after SALB injection. To test the effects of nor-BNI on mechanical hypersensitivity, nor-BNI (1 μg in 10 μl PBS) was intrathecally injected into WT mice and mechanical hypersensitivity was measured before injection and at 60 min after injection.

Intraspinal Virus Injection—Plasmid pAAV-hSyn-dF-HA-KORD-IRES mCitrine (Addgene) were packaged in serotype AAV2/8 in the Boston Children's Hospital Viral Core. The virus titer is 1.026E+15gc/ml. Animals were anesthetized with ketamine/xylazine (in combination at 150 mg/kg ketamine and 5 mg/kg xylazine in 0.2 ml saline) and then mounted to the stereotaxic frame. The vertebral lamina and dorsal spinous process were removed at L4–L5 level. After dural removal, virus was injected at the position 500 μm left to the dorsal blood vessel at a depth of 250 μm using a glass micropipette attached to a 10 μl Hamilton syringe. Virus was injected at 3 points 1 mm interspaced and 500 nl per point. The micropipette was left in place for 5 min to increase diffusion after each injection. Incision in the lumbar spinal cord was closed with stitches and buprenorphine (0.05 mg/kg) was applied twice subcutaneously in the back of mice, with the 12-hour interval, to reduce post-surgery suffering. For animals used for behavioral studies, viral injections were performed at adult stages (1.5–2.5-month old). For electrophysiological recordings, viral injections were

performed at P3–P7. Behavioral testing or slice recording was performed 3 weeks after virus injection.

Spinal Cord Slice Preparation—Parasagittal spinal cord slices with attached dorsal root (8–18 mm) and DRG were prepared as described previously (Cheng et al., 2017; Duan et al., 2014). In brief, mice (P24–P31) were deeply anesthetized with isoflurane and decapitated, and the lumbar spinal cord was quickly removed to ice-cold modified artificial cerebrospinal fluid (ACSF) (cutting solution), which contains (in mM): 80 NaCl, 2.5 KCl, 1.25 NaH_2PO_4, 0.5 $CaCl_2$, 3.5 $MgCl_2$, 25 $NaHCO_3$, 75 sucrose, 1.3 sodium ascorbate and 3.0 sodium pyruvate, with pH 7.4 and osmolality 310–320 mOsm. The spinal cord with attached dorsal roots and DRG was cut parasagittally (350–500 μm) by VT1000S vibratome (Leica, Germany). Slices were incubated for about 1 h at 33 °C in a recording solution containing (in mM) 125 NaCl, 2.5 KCl, 2 $CaCl_2$, 1 $MgCl_2$, 1.25 NaH_2PO4, 26 $NaHCO_3$, 25 d-glucose, 1.3 sodium ascorbate and 3.0 sodium pyruvate, with pH at 7.2 and measured osmolality at 310–320 mOsm, and the solution was oxygenated with 95% O_2 and 5% CO_2. Individual slices were then transferred into a recording chamber and perfused with oxygenated recording solution at 5 ml/min during electrophysiological recordings at room temperature (25°C).

Patch-clamp Recordings and Dorsal Root Stimulation—Whole-cell recording experiments were conducted as described previously (Cheng et al., 2017; Duan et al., 2014). Recordings were made from SOM^{Cre}-$tdTomato^+$, SOM^{Cre}-negative, $Pdyn^{Cre}$-$tdTomato^+$, $Pdyn^{Cre}$-negative, $VGAT^{Cre}$-$tdTomato^+$ or randomly picked neurons in the lamina I and II_o. To determine the percentage of neurons in the lamina I and II_o that are SOM^{Cre}-$tdTomato^+$, we made the random picking of neuronal cells under the bright field, and then checked tdTomato expression under the fluorescent channel. The internal solution contains (in mM): potassium gluconate 130, KCl 5, Na2ATP 4, NaGTP 0.5, HEPES 20, EGTA 0.5, pH 7.28 with KOH, and measured osmolality at 310–320 mOsm. Data were acquired with pClamp 10.0 software (Molecular Devices, USA) using MultiClamp 700B patch-clamp amplifier and Digidata 1440A (Molecular Devices). Responses were low-pass filtered on-line at 2 kHz, and digitized at 5 kHz.

25 μA (pulse widths 0.1 ms) was used to screen for Aβ fiber-mediated synaptic inputs/outputs in the spinal dorsal horn. The distance from the tip of the stimulation electrode to the entrance of the attached dorsal root is around 8 mm. We recorded the response under three different conditions to test primary afferent inputs to dorsal horn neurons. First, by holding membrane potential at −70 mV, evoked inhibitory postsynaptic currents (eIPSCs) were attenuated (Yoshimura and Jessell, 1990), such that even small evoked excitatory postsynaptic currents (eEPSCs) could be detected, although we should recognize that recorded eEPSCs will be distorted by activation of voltage-dependent channels, particularly in spines and distal dendrites due to voltage clamp failure (Beaulieu-Laroche and Harnett, 2018; Williams and Mitchell, 2008). This recording condition was used to study whether a neuron received inputs directly (monosynaptic) or indirectly (polysynaptic) from Aβ fibers, as well as to measure the latencies of eEPSCs. Latencies were determined by the intervals between the stimulation artifact and the beginning of detectable eEPSC, eIPSC and eAP.

Because of the weak stimulation intensity (25 μA), the artifact is very small, but can still be seen after the trace was enlarged. Monosynaptic Aβ inputs were determined by following 20 Hz stimulation without failure with latency variations < 0.5 ms (Cheng et al., 2017). Second, by holding the membrane potential at 0 mV and including QX-314 (5 mM, Sigma-Aldrich) into the internal solution of the recording electrode, eEPSCs were minimized and eIPSCs could be more easily detected, such that the latency to the onset of eIPSCs could be measured accordingly. Third, to record dorsal root stimulation-evoked APs (Aβ-evoked APs), current-clamp recordings were performed without current injection; for those few neurons with spontaneous firing, current injection was performed to keep the membrane potential slightly hyperpolarized to block the generation of spontaneous AP firings. The recordings were performed either under the normal recording solution or under the disinhibition condition with the presence of both bicuculline (10 μM) and strychnine (2 μM). To detect spontaneous AP firings, the neuron was recorded without any current injection. AP firing patterns following current injections were determined under the conditions with the membrane potentials held around −85 mV. To manipulate potassium channels and NMDARs in the recorded neurons, 4-AP (2 mM) and MK-801 (2 mM) were freshly prepared and included into the internal solution of the recording electrode. To test the effects of intra plantar capsaicin injection on Aβ-evoked EPSCs/APs or A currents, the slices were prepared 1 hour after capsaicin injection. To test effects of the MEK inhibitor PD98059 on capsaicin-induced firing or on size changes of A currents, PD98059 (0.5 μg, 10 μl, 10% DMSO) or the vehicle (10 μl, 10% DMSO) was intrathecally injected and flushed with 10 μl of saline. After 30 min, capsaicin was intradermally injected into the plantar region of the left hindpaw and mice were killed for analysis one hour later. To test acute silencing of $Pdyn^{Cre}$ neurons on Aβ-evoked EPSCs/APs, the slices were prepared from mice 3 weeks after intraspinal virus injection, and SALB (500 nM) was bath applied during the recording. To test the effects of nor-BNI (1 μM) on Aβ-evoked EPSCs/APs, the slices were pretreated with nor-BNI for at least 30 min before recording.

The external solution for the I_A current recordings is Ca^{2+}-free ACSF containing (in mM) 80 NaCl, 2.5 KCl, 1.25 NaH_2PO4, 3 $MgCl_2$, 25 $NaHCO_3$, 75 sucrose, 1.3 sodium ascorbate, 3.0 sodium pyruvate and 500 nM TTX (tetrodotoxin) to block voltage-gated Na^+ currents, Ca^{2+} currents, and Ca^{2+}-activated K^+ currents. Both the capacitance and series resistance were well compensated. To record I_A current, a two-step voltage protocol was used (Hu et al., 2006), under the guidance of our colleague Dr. Bruce Bean. The first step was to determine the total outward current, and voltage steps of 500 ms pulses stepping from −80 mV to +40 mV were applied at 5 s intervals. To determine the sustained current, conditioning pre-pulses ranging from −80 mV to −10 mV were applied for 150 ms to inactivate transient potassium channels and then followed by a step to +40 mV for 500 ms at 5 s intervals. Subtraction of the sustained current from the total current isolated the A-type current. Series resistances for all neurons recorded in this study were within 30 mΩ, and the liquid junction potentials were 17.8 mV and were corrected off-line for resting membrane potential (RMP) measurement. As such, the corrected RMPs reported here are different from those uncorrected RMPs we reported previously (Cheng et al., 2017).

Immunohistochemistry—Immunohistochemistry procedure was conducted as described previously (Cheng et al., 2017). Spinal cord sections were performed using rabbit anti-c-Fos (1: 500, Millipore, ABE457), rabbit anti-pERK (1: 500, Cell signaling technology, 4370S) or rabbit anti-GFP (1: 500, ThermoFisher Scientific, A-11122) diluted in 0.3% Triton X-100 plus 10% normal goat serum in PBS, and goat anti-rabbit (1:500, Invitrogen, A11034) diluted in 0.3% Triton X-100 in PBS.

QUANTIFICATION AND STATTISTICAL ANALYSIS

Results were represented as means ± S.E.M. except I_A and I_D. Results for I_A and I_D were represented as interquartile range (Q1–Q3 with median denoted in between). The outlier data of I_A and I_D were identified by the +/− 3 standard deviations. Statistical analyses were done using GraphPad Prism. For capsaicin-induced acute licking, nor-BNI-induced mechanical hypersensitivity, and t_{EPSC}, t_{IPSC}, t_{AP} assessment, data were subjected to Student's t tests. For I_A and I_D assessment, data were subjected to Mann-Whitney Rank Sum Test. For mechanical hypersensitivity induced by capsaicin or following acute silencing of *Pdyn*-Cre neurons, time-course measurements were assessed by Two-way ANOVA with Holm-sidak test. For statistical analysis of incidence of electrophysiological results, data were analyzed with chi-squared ($\chi 2$) tests. $p < 0.05$ was accepted as significant changes.

Supplementary Material

Refer to Web version on PubMed Central for supplementary material.

ACKNOWLEDGMENTS

We thank Dr. Josh Huang and the Jackson laboratory for the *Somatostatin-IRES-Cre* (*SOM*^{Cre}) mice, Dr. Bradford B. Lowell for the *Vglut3*^{Cre}, *Preprodynorphin-IRES-Cre* (*Pdyn*^{Cre}), and *Vgat-IRES-Cre* (*GAT*^{Cre}) mice, and the Allen Brain Institute/the Jackson Laboratory for the *ROSA26-lsl-tdTomato* mice. We thank Dr. Bo Duan for performing part of behavioral analyses, Dr. Longzhen Cheng for analyzing Aβ-evoked firing latencies in Pdyn^{Cre}-ablated mice, and Dr. Shing-Hong Lin for spinal virus injection. We thank Dr. Bruce Bean and Dr. Wenqin Hu for the meticulous advice on recording I_A currents and for their critical comments on the manuscript. We also thank Dr. Clifford Woolf and Dr. Bernardo Sabatini for helpful discussions. The work was supported by NIH grants to Q.M. (R01 DE018025) and to Q.M. and M.G. (R01 NS086372). Y.Z. was supported by Grants from National Natural Science Fund of China (31300922), 2016 Postdoctoral International Exchange Program of China and Development Project of Shanghai Peak Disciplines-Integrated Medicine (20150407). S.L. was supported by Grants from National Natural Science Fund of China (KRF2640065) and The China Postdoctoral Science Foundation (KLF101846).

REFERENCES

Adams JP, Anderson AE, Varga AW, Dineley KT, Cook RG, Pfaffinger PJ, and Sweatt JD (2000). The A-type potassium channel Kv4.2 is a substrate for the mitogen-activated protein kinase ERK. J. Neurochem 75, 2277–2287. [PubMed: 11080179]

Armstrong CM, and Gilly WF (1992). Access resistance and space clamp problems associated with whole-cell patch clamping. Methods Enzymol 207, 100–122. [PubMed: 1528114]

Baba H, Ji RR, Kohno T, Moore KA, Ataka T, Wakai A, Okamoto M, and Woolf CJ (2003). Removal of GABAergic inhibition facilitates polysynaptic A fiber-mediated excitatory transmission to the superficial spinal dorsal horn. Mol. Cell Neurosci 24, 818–830. [PubMed: 14664828]

Bardoni R, Magherini PC, and MacDermott AB (1998). NMDA EPSCs at glutamatergic synapses in the spinal cord dorsal horn of the postnatal rat. J. Neurosci 18, 6558–6567. [PubMed: 9698343]

Beaulieu-Laroche L, and Harnett MT (2018). Dendritic Spines Prevent Synaptic Voltage Clamp. Neuron 97, 75–82. [PubMed: 29249288]

Bessou P, and Perl ER (1969). Response of cutaneous sensory units with unmyelinated fibers to noxious stimuli. J. Neurophysiol 32, 1025–1043. [PubMed: 5347705]

Binshtok AM, Bean BP, and Woolf CJ (2007). Inhibition of nociceptors by TRPV1-mediated entry of impermeant sodium channel blockers. Nature 449, 607–610. [PubMed: 17914397]

Bloodgood BL, and Sabatini BL (2008). Regulation of synaptic signalling by postsynaptic, non-glutamate receptor ion channels. J. Physiol 586, 1475–1480. [PubMed: 18096597]

Boada MD, and Woodbury CJ (2008). Myelinated skin sensory neurons project extensively throughout adult mouse substantia gelatinosa. J. Neurosci 28, 2006–2014. [PubMed: 18305235]

Bonin RP, and De Koninck Y (2013). Restoring ionotropic inhibition as an analgesic strategy. Neurosci. Lett 557 Pt A, 43–51. [PubMed: 24080373]

Bourane S, Duan B, Koch SC, Dalet A, Britz O, Garcia-Campmany L, Kim E, Cheng L, Ghosh A, Ma Q, et al. (2015a). Gate control of mechanical itch by a subpopulation of spinal cord interneurons. Science 350, 550–554. [PubMed: 26516282]

Bourane S, Grossmann KS, Britz O, Dalet A, Del Barrio MG, Stam FJ, Garcia-Campmany L, Koch S, and Goulding M (2015b). Identification of a spinal circuit for light touch and fine motor control. Cell 160, 503–515. [PubMed: 25635458]

Braz J, Solorzano C, Wang X, and Basbaum AI (2014). Transmitting pain and itch messages: a contemporary view of the spinal cord circuits that generate gate control. Neuron 82, 522–536. [PubMed: 24811377]

Cameron D, Polgar E, Gutierrez-Mecinas M, Gomez-Lima M, Watanabe M, and Todd AJ (2015). The organisation of spinoparabrachial neurons in the mouse. Pain 156, 2061–2071. [PubMed: 26101837]

Chaplan SR, Bach FW, Pogrel JW, Chung JM, and Yaksh TL (1994). Quantitative assessment of tactile allodynia in the rat paw. J. Neurosci. Meth 53, 55–63.

Cheng L, Duan B, Huang T, Zhang Y, Chen Y, Britz O, Garcia-Campmany L, Ren X, Vong L, Lowell BB, et al. (2017). Identification of spinal circuits involved in touch-evoked dynamic mechanical pain. Nat. Neurosci 20, 804–814. [PubMed: 28436981]

Chiu CQ, Lur G, Morse TM, Carnevale NT, Ellis-Davies GC, and Higley MJ (2013). Compartmentalization of GABAergic inhibition by dendritic spines. Science 340, 759–762. [PubMed: 23661763]

Cordero-Erausquin M, Allard S, Dolique T, Bachand K, Ribeiro-da-Silva A, and De Koninck Y (2009). Dorsal horn neurons presynaptic to lamina I spinoparabrachial neurons revealed by transynaptic labeling. J. Comp. Neurol 517, 601–615. [PubMed: 19824098]

Cui L, Miao X, Liang L, Abdus-Saboor I, Olson W, Fleming MS, Ma M, Tao YX, and Luo W (2016). Identification of Early RET+ Deep Dorsal Spinal Cord Interneurons in Gating Pain. Neuron 91, 1137–1153. [PubMed: 27545714]

Duan B, Cheng L, Bourane S, Britz O, Padilla C, Garcia-Campmany L, Krashes M, Knowlton W, Velasquez T, Ren X, et al. (2014). Identification of spinal circuits transmitting and gating mechanical pain. Cell 159, 1417–1432. [PubMed: 25467445]

Duan B, Cheng L, and Ma Q (2018). Spinal Circuits Transmitting Mechanical Pain and Itch. Neurosci. Bull 34:186–193. [PubMed: 28484964]

Edmonds B, Gibb AJ, and Colquhoun D (1995). Mechanisms of activation of glutamate receptors and the time course of excitatory synaptic currents. Annu. Rev. Physiol 57, 495–519. [PubMed: 7778875]

Foster E, Wildner H, Tudeau L, Haueter S, Ralvenius WT, Jegen M, Johannssen H, Hösli L, Haenraets K, Ghanem A, et al. (2015). Targeted ablation, silencing, and activation establish glycinergic dorsal horn neurons as key components of a spinal gate for pain and itch. Neuron 85, 1289–1304. [PubMed: 25789756]

Gobel S, and Dubner R (1969). Fine structural studies of the main sensory trigeminal nucleus in the cat and rat. J. Comp. Neurol 137, 459–493. [PubMed: 5361245]

Gobel S (1978). Golgi studies of the neurons in layer II of the dorsal horn of the medulla (trigeminal nucleus caudalis). J. Comp. Neurol 180, 395–413. [PubMed: 659668]

Gutierrez-Mecinas M, Furuta T, Watanabe M, and Todd AJ (2016). A quantitative study of neurochemically defined excitatory interneuron populations in laminae I-III of the mouse spinal cord. Mol. Pain 12, 1–18.

Harnett MT, Xu NL, Magee JC, and Williams SR (2013). Potassium channels control the interaction between active dendritic integration compartments in layer 5 cortical pyramidal neurons. Neuron 79, 516–529. [PubMed: 23931999]

Hoffman DA, Magee JC, Colbert CM, and Johnston D (1997). K+ channel regulation of signal propagation in dendrites of hippocampal pyramidal neurons. Nature 387, 869–875. [PubMed: 9202119]

Hu HJ, Alter BJ, Carrasquillo Y, Qiu CS, and Gereau R.W.t. (2007). Metabotropic glutamate receptor 5 modulates nociceptive plasticity via extracellular signal-regulated kinase-Kv4.2 signaling in spinal cord dorsal horn neurons. J. Neurosci 27, 13181–13191. [PubMed: 18045912]

Hu HJ, Carrasquillo Y, Karim F, Jung WE, Nerbonne JM, Schwarz TL, and Gereau R.W.t. (2006). The Kv4.2 potassium channel subunit is required for pain plasticity. Neuron 50, 89–100. [PubMed: 16600858]

Hu HJ, Glauner KS, and Gereau R.W.t. (2003). ERK integrates PKA and PKC signaling in superficial dorsal horn neurons. I. Modulation of A-type K+ currents. J. Neurophysiol 90, 1671–1679. [PubMed: 12750419]

Huang HY, Cheng JK, Shih YH, Chen PH, Wang CL, and Tsaur ML (2005). Expression of A-type K channel alpha subunits Kv 4.2 and Kv 4.3 in rat spinal lamina II excitatory interneurons and colocalization with pain-modulating molecules. Eur. J. Neurosci 22, 1149–1157. [PubMed: 16176357]

Huang J, Polgar E, Solinski HJ, Mishra SK, Tseng PY, Iwagaki N, Boyle KA, Dickie AC, Kriegbaum MC, Wildner H, et al. (2018). Circuit dissection of the role of somatostatin in itch and pain. Nat. Neurosci 21, 707–716. [PubMed: 29556030]

Huettner JE, and Bean BP (1988). Block of N-methyl-D-aspartate-activated current by the anticonvulsant MK-801: selective binding to open channels. PNAS 85, 1307–1311. [PubMed: 2448800]

Ji RR, Baba H, Brenner GJ, and Woolf CJ (1999). Nociceptive-specific activation of ERK in spinal neurons contributes to pain hypersensitivity. Nat. Neurosci 2, 1114–1119. [PubMed: 10570489]

Jin SX, Zhuang ZY, Woolf CJ, and Ji RR (2003). p38 mitogen-activated protein kinase is activated after a spinal nerve ligation in spinal cord microglia and dorsal root ganglion neurons and contributes to the generation of neuropathic pain. J. Neurosci 23, 4017–4022. [PubMed: 12764087]

Julius D (2013). TRP channels and pain. Annu. Rev. Cell Dev. Biol 29, 355–384. [PubMed: 24099085]

Kardon AP, Polgar E, Hachisuka J, Snyder LM, Cameron D, Savage S, Cai X, Karnup S, Fan CR, Hemenway GM, et al. (2014). Dynorphin acts as a neuromodulator to inhibit itch in the dorsal horn of the spinal cord. Neuron 82, 573–586. [PubMed: 24726382]

Kerchner GA, and Nicoll RA (2008). Silent synapses and the emergence of a postsynaptic mechanism for LTP. Nat. Rev 9, 813–825.

Koltzenburg M, Lundberg LE, and Torebjork HE (1992). Dynamic and static components of mechanical hyperalgesia in human hairy skin. Pain 51, 207–219. [PubMed: 1484717]

Kopach O, Kao SC, Petralia RS, Belan P, Tao YX, and Voitenko N (2011). Inflammation alters trafficking of extrasynaptic AMPA receptors in tonically firing lamina II neurons of the rat spinal dorsal horn. Pain 152, 912–923. [PubMed: 21282008]

Krashes MJ, Shah BP, Madara JC, Olson DP, Strochlic DE, Garfield AS, Vong L, Pei H, Watabe-Uchida M, Uchida N, et al. (2014). An excitatory paraventricular nucleus to AgRP neuron circuit that drives hunger. Nature 507, 238–242. [PubMed: 24487620]

Latremoliere A, and Woolf CJ (2009). Central sensitization: a generator of pain hypersensitivity by central neural plasticity. J. Pain 10, 895–926. [PubMed: 19712899]

Lee DZ, Chung JM, Chung K, and Kang MG (2012). Reactive oxygen species (ROS) modulate AMPA receptor phosphorylation and cell-surface localization in concert with pain-related behavior. Pain 153, 1905–1915. [PubMed: 22770842]

Lewis T (1936). Experiments relating to cutaneous hyperalgesia and its spread through somatic nerves. Clin. Sci 2, 373–423.

Li P, and Zhuo M (1998). Silent glutamatergic synapses and nociception in mammalian spinal cord. Nature 393, 695–698. [PubMed: 9641681]

Lin Q, Peng YB, and Willis WD (1996). Inhibition of primate spinothalamic tract neurons by spinal glycine and GABA is reduced during central sensitization. J. Neurophysiol 76, 1005–1014. [PubMed: 8871215]

Lu Y, Dong H, Gao Y, Gong Y, Ren Y, Gu N, Zhou S, Xia N, Sun YY, Ji RR, et al. (2013). A feed-forward spinal cord glycinergic neural circuit gates mechanical allodynia. J. Clin. Invest 123, 4050–4062. [PubMed: 23979158]

Madisen L, Zwingman TA, Sunkin SM, Oh SW, Zariwala HA, Gu H, Ng LL, Palmiter RD, Hawrylycz MJ, Jones AR, et al. (2010). A robust and high-throughput Cre reporting and characterization system for the whole mouse brain. Nat. Neurosci 13, 133–140. [PubMed: 20023653]

Major G, Larkum ME, and Schiller J (2013). Active properties of neocortical pyramidal neuron dendrites. Annu. Rev. Neurosci 36, 1–24. [PubMed: 23841837]

Melzack R, and Wall PD (1965). Pain mechanisms: a new theory. Science 150, 971–979. [PubMed: 5320816]

Mendell LM (2014). Constructing and deconstructing the gate theory of pain. Pain 155, 210–216. [PubMed: 24334188]

Merrill EG, and Wall PD (1972). Factors forming the edge of a receptive field: the presence of relatively ineffective afferent terminals. J. Physiol 226, 825–846. [PubMed: 4637631]

Nimchinsky EA, Sabatini BL, and Svoboda K (2002). Structure and function of dendritic spines. Annu. Rev. Physiol 64, 313–353. [PubMed: 11826272]

Peirs C, Williams SP, Zhao X, Walsh CE, Gedeon JY, Cagle NE, Goldring AC, Hioki H, Liu Z, Marell PS, et al. (2015). Dorsal Horn Circuits for Persistent Mechanical Pain. Neuron 87, 797–812. [PubMed: 26291162]

Petitjean H, Pawlowski SA, Fraine SL, Sharif B, Hamad D, Fatima T, Berg J, Brown CM, Jan LY, Ribeiro-da-Silva A, et al. (2015). Dorsal Horn Parvalbumin Neurons Are Gate-Keepers of Touch-Evoked Pain after Nerve Injury. Cell Rep 13, 1246–1257. [PubMed: 26527000]

Petralia RS, Esteban JA, Wang YX, Partridge JG, Zhao HM, Wenthold RJ, and Malinow R (1999). Selective acquisition of AMPA receptors over postnatal development suggests a molecular basis for silent synapses. Nat. Neurosci 2, 31–36. [PubMed: 10195177]

Polgar E, Hughes DI, Riddell JS, Maxwell DJ, Puskar Z, and Todd AJ (2003). Selective loss of spinal GABAergic or glycinergic neurons is not necessary for development of thermal hyperalgesia in the chronic constriction injury model of neuropathic pain. Pain 104, 229–239. [PubMed: 12855333]

Polgar E, Sardella TC, Tiong SY, Locke S, Watanaabe M, and Todd AJ (2013). Functional differences between neurochemically defined populations of inhibitory interneurons in the rat spinal dorsal horn. Pain 154, 2606–2615. [PubMed: 23707280]

Portoghese PS, Lipkowski AW, and Takemori AE (1987). Binaltorphimine and nor-binaltorphimine, potent and selective kappa-opioid receptor antagonists. Life Sci 40, 1287–1292. [PubMed: 2882399]

Prescott SA (2015). Synaptic inhibition and disinhibition in the spinal dorsal horn. Prog. Mol. Biol. Transl. Sci 131, 359–383. [PubMed: 25744679]

Shibata R, Nakahira K, Shibasaki K, Wakazono Y, Imoto K, and Ikenaka K (2000). A-type K+ current mediated by the Kv4 channel regulates the generation of action potential in developing cerebellar granule cells. J. Neurosci 20, 4145–4155. [PubMed: 10818150]

Spike RC, Puskar Z, Andrew D, and Todd AJ (2003). A quantitative and morphological study of projection neurons in lamina I of the rat lumbar spinal cord. Eur. J. Neurosci 18, 2433–2448. [PubMed: 14622144]

Stuart GJ, and Spruston N (2015). Dendritic integration: 60 years of progress. Nat. Neurosci 18, 1713–1721. [PubMed: 26605882]

Takazawa T, Choudhury P, Tong CK, Conway CM, Scherrer G, Flood PD, Mukai J, and MacDermott AB (2017). Inhibition Mediated by Glycinergic and GABAergic Receptors on Excitatory Neurons

in Mouse Superficial Dorsal Horn Is Location-Specific but Modified by Inflammation. J. Neurosci 37, 2336–2348. [PubMed: 28130358]

Takazawa T, and MacDermott AB (2010). Synaptic pathways and inhibitory gates in the spinal cord dorsl horn. Ann. N. Y. Acad. Sci 1198, 153–158. [PubMed: 20536929]

Taniguchi H, He M, Wu P, Kim S, Paik R, Sugino K, Kvitsiani D, Fu Y, Lu J, Lin Y, et al. (2011). A resource of Cre driver lines for genetic targeting of GABAergic neurons in cerebral cortex. Neuron 71, 995–1013. [PubMed: 21943598]

Tao YX (2012). AMPA receptor trafficking in inflammation-induced dorsal horn central sensitization. Neurosci. Bull 28, 111–120. [PubMed: 22466122]

Todd AJ (2010). Neuronal circuitry for pain processing in the dorsal horn. Nat. Rev. Neurosci 11, 823–836. [PubMed: 21068766]

Torebjork HE, Lundberg LE, and LaMotte RH (1992). Central changes in processing of mechanoreceptive input in capsaicin-induced secondary hyperalgesia in humans. J. Physiol 448, 765–780. [PubMed: 1593489]

Torsney C, and MacDermott AB (2006). Disinhibition opens the gate to pathological pain signaling in superficial neurokinin 1 receptor-expressing neurons in rat spinal cord. J. Neurosci 26, 1833–1843. [PubMed: 16467532]

Trimmer JS (2015). Subcellular localization of K+ channels in mammalian brain neurons: remarkable precision in the midst of extraordinary complexity. Neuron 85, 238–256. [PubMed: 25611506]

Vardy E, Robinson JE, Li C, Olsen RHJ, DiBerto JF, Giguere PM, Sassano FM, Huang XP, Zhu H, Urban DJ, et al. (2015). A New DREADD Facilitates the Multiplexed Chemogenetic Interrogation of Behavior. Neuron 86, 936–946. [PubMed: 25937170]

Vilardaga JP, Bunemann M, Krasel C, Castro M, and Lohse MJ (2003). Measurement of the millisecond activation switch of G protein-coupled receptors in living cells. Nat. Biotechnol 21, 807–812. [PubMed: 12808462]

Vong L, Ye C, Yang Z, Choi B, Chua S, Jr., and Lowell BB (2011). Leptin action on GABAergic neurons prevents obesity and reduces inhibitory tone to POMC neurons. Neuron 71, 142–154. [PubMed: 21745644]

Williams SR, and Mitchell SJ (2008). Direct measurement of somatic voltage clamp errors in central neurons. Nat. Neurosci 11, 790–798. [PubMed: 18552844]

Yoshimura M, and Jessell T (1990). Amino acid-mediated EPSPs at primary afferent synapses with substantia gelatinosa neurones in the rat spinal cord. J. Physiol 430, 315–335. [PubMed: 1982314]

Zeilhofer HU, Wildner H, and Yevenes GE (2012). Fast synaptic inhibition in spinal sensory processing and pain control. Physiol. Rev 92, 193–235. [PubMed: 22298656]

Highlights:

- Reliance on NMDARs for firing solves timing problems of feedforward inhibition
- Electric filtering including I_A currents sets up a permissive condition
- Pdyn^{Cre}-derived inhibitory neurons constitutively establish the sizes of I_A
- Strong nociceptor inputs open the gate partly by attenuating I_A

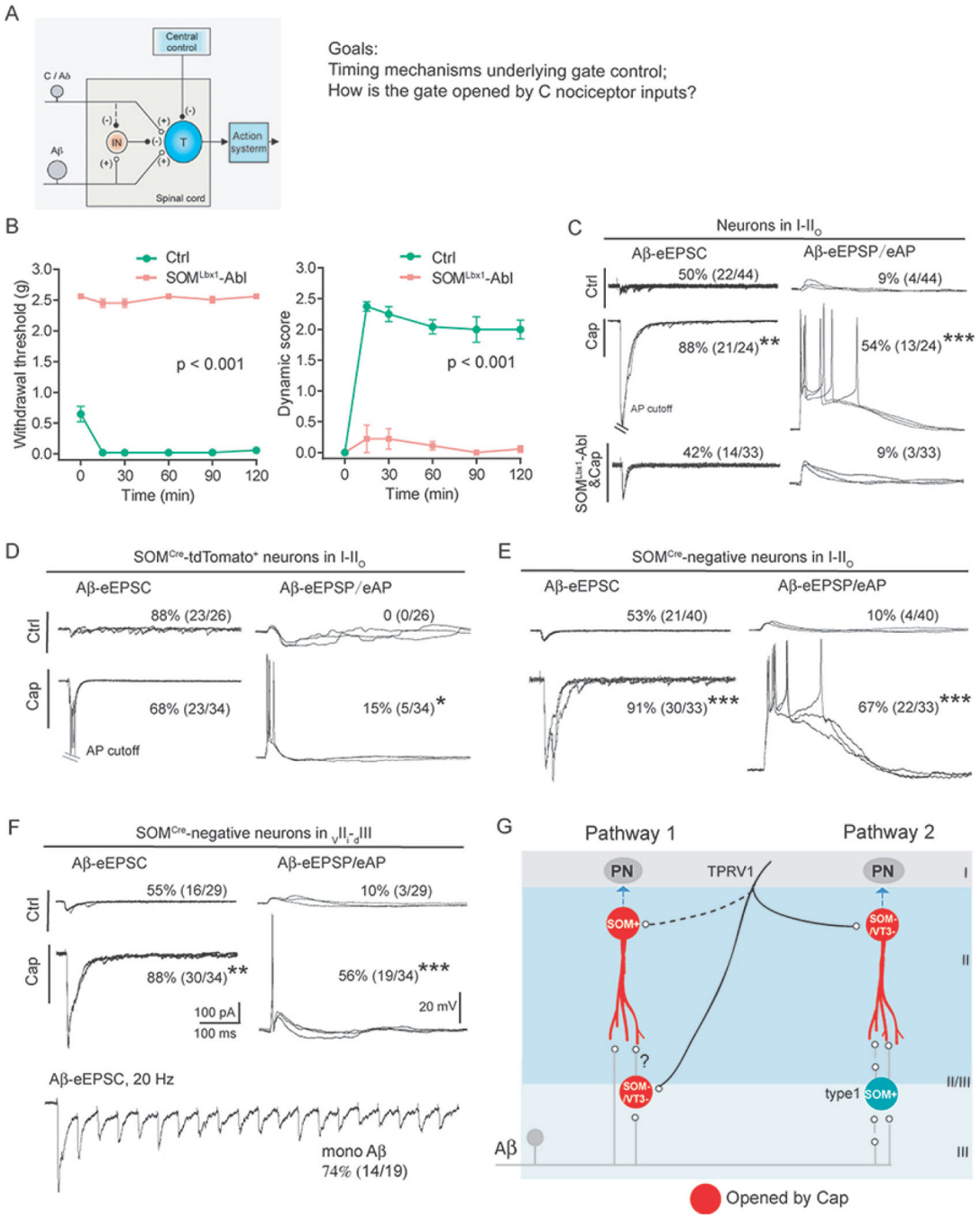

Figure 1. The roles of SOM^{Cre}-derived and SOM^{Cre}-negative neurons in transmitting capsaicin-induced mechanical hypersensitivity

(A) Schematic description of the modified gate control theory and two-related goals in this study. “T” represents a spinal transmission neuron. “IN”: an inhibitory neuron. “(+)” and “(−)” represent excitatory and inhibitory inputs, respectively. The dashed line indicates that C/Aδ fibers might activate an unknown pathway to inactivate IN, a key tenet to be tested in this study.

(B) Loss of capsaicin-induced von-Frey filament-evoked punctate mechanical hypersensitivity in SOM^{Lbx1}-ablated mice (“SOM^{Lbx1}-Abl”, n = 8) in comparison with

control littermates ("Ctrl", n = 6) ($F_{(1, 12)}$ = 6365.07, ***p < 0.001, two-way ANOVA), and loss of brush-evoked dynamic hypersensitivity ($F_{(1, 12)}$ = 212.753, ***p < 0.001, two-way ANOVA).

(C) Representative traces of Aβ-evoked inputs (left) and outputs (right) in neurons within I-II_o of wild type mice without treatment ("Ctrl") or with hindpaw capsaicin injection ("Cap"), and capsaicin-injected SOM^{Lbx1}-Abl mice ("SOM^{Lbx1}-Abl&Cap").

(D-F) Representative traces of Aβ-evoked inputs (left) and outputs (right) in SOM^{Cre}-$tdTomato^{+}$ neurons in I-II_o (D), or SOM^{Cre}-negative neurons in I-II_o (E) or in $_{v}II_{i}$-$_{d}III$ (F). Recordings were done in slices from mice treated with capsaicin (bottom, "cap") or not (top, "Ctrl"). Aβ inputs indicated by Aβ-eEPSCs at −70 mV with voltage clamp; Aβ outputs indicated by Aβ-eEPSPs and eAPs with current clamp. Bottom in (F): Aβ-eEPSCs following 20 Hz stimulation, indicating monosynaptic inputs ("mono Aβ").

(G) Schematic description of two pathways relaying Aβ inputs to superficial dorsal horn neurons following hindpaw capsaicin injection. Red circles show neurons sensitized by capsaicin. "SOM+" for SOM^{Cre}-derived neurons, "SOM-/VT3-" for neurons double negative for both SOM^{Cre} and $VGLUT3^{Cre}$. All recordings (C-F, except the bottom trace in F) are composed of three traces at 0.033 Hz. Data in B are presented as means ± S.E.M.. See also Figures S1 and S2.

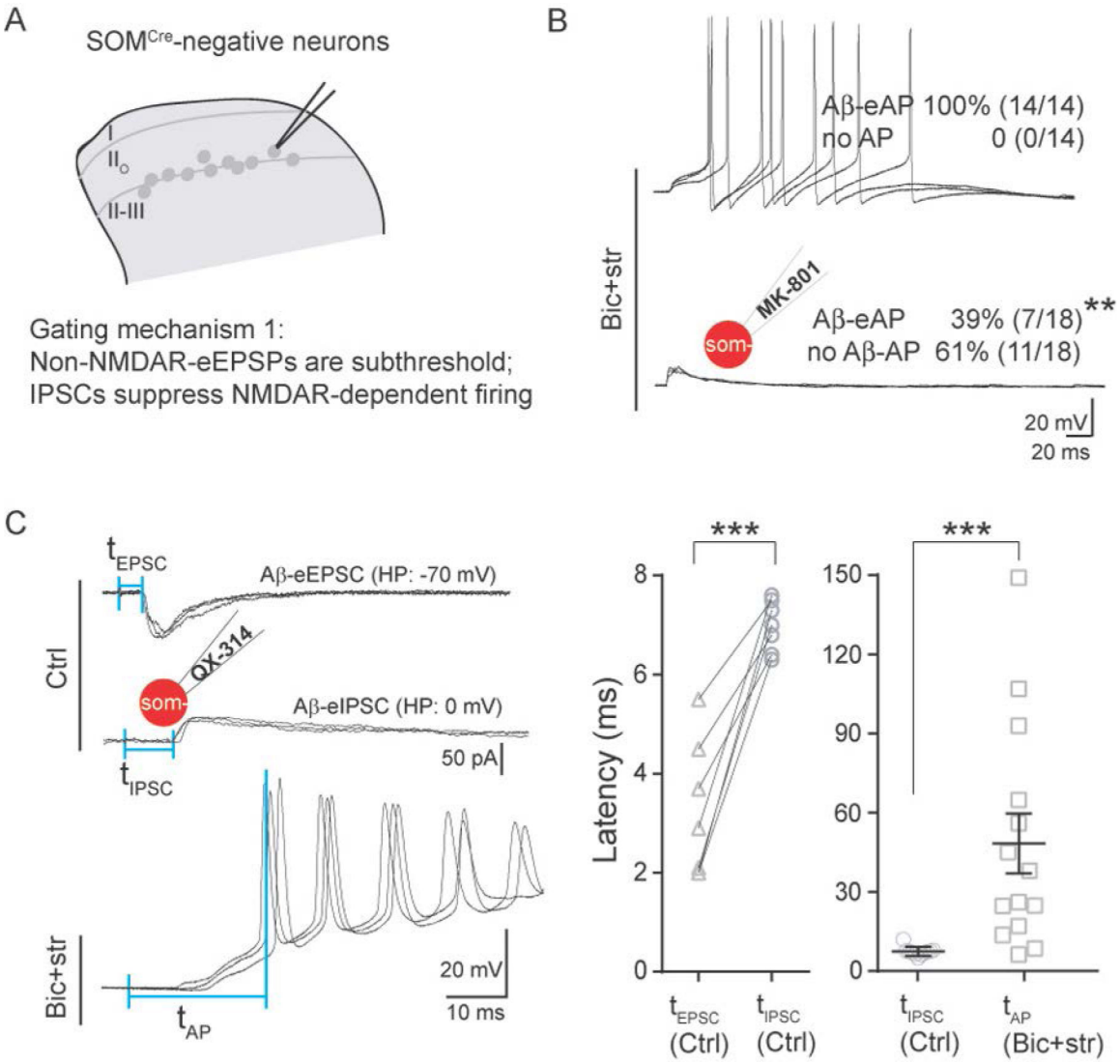

Figure 2. Latencies of Aβ-evoked EPSC, IPSC and NMDAR-dependent firing in SOM^{Cre}-negative neurons within $_{v}II_{i}$-$_{d}III$

(A) Schematic showing of recorded SOM^{Cre}-negative neurons and the proposed gating mechanism 1.

(B) Representative traces of Aβ-evoked outputs in SOM^{Cre}-negative neurons under the disinhibition condition with bicuculline (10 μM) plus strychnine (2 μM) (“Bic+str”), or combined with intracellular MK-801. MK-801 blocked most Aβ-evoked AP firing (“Aβ-eAP”, Chi-square test, **p < 0.01).

(C) Timing of Aβ-evoked excitatory and inhibitory inputs and outputs. Left: typical traces of Aβ-eEPSCs and Aβ-eIPSCs under the normal ACSF recording condition (“Ctrl”) and Aβ-eAPs under the disinhibition condition (“Bic+str”). The first and second vertical blue lines represent the stimulation artifact and the beginning of detectable eEPSC, eIPSC and eAP. The latencies, defined by the intervals of these two vertical blue lines, were referred to as t_{EPSC}, t_{IPSC} and t_{AP}, respectively. Middle: t_{EPSC} was shorter than t_{IPSC} in the same neurons (“t_{EPSC}, Ctrl” and “t_{IPSC}, Ctrl”, respectively; paired t test, ***p < 0.001). Right: t_{IPSC} under

the normal condition ("t_{IPSC}, Ctrl") was shorter than t_{AP} with Bic+str ("t_{AP}, Bic+str") (two-tailed Student's unpaired test, ***$p < 0.001$).

The insets of the schematic recording electrode indicate intracellular application of QX-314 (5 mM) or MK-801 (2 mM). All shown recordings (B-C) are composed of three traces at 0.033 Hz. Data are represented as means ± S.E.M.

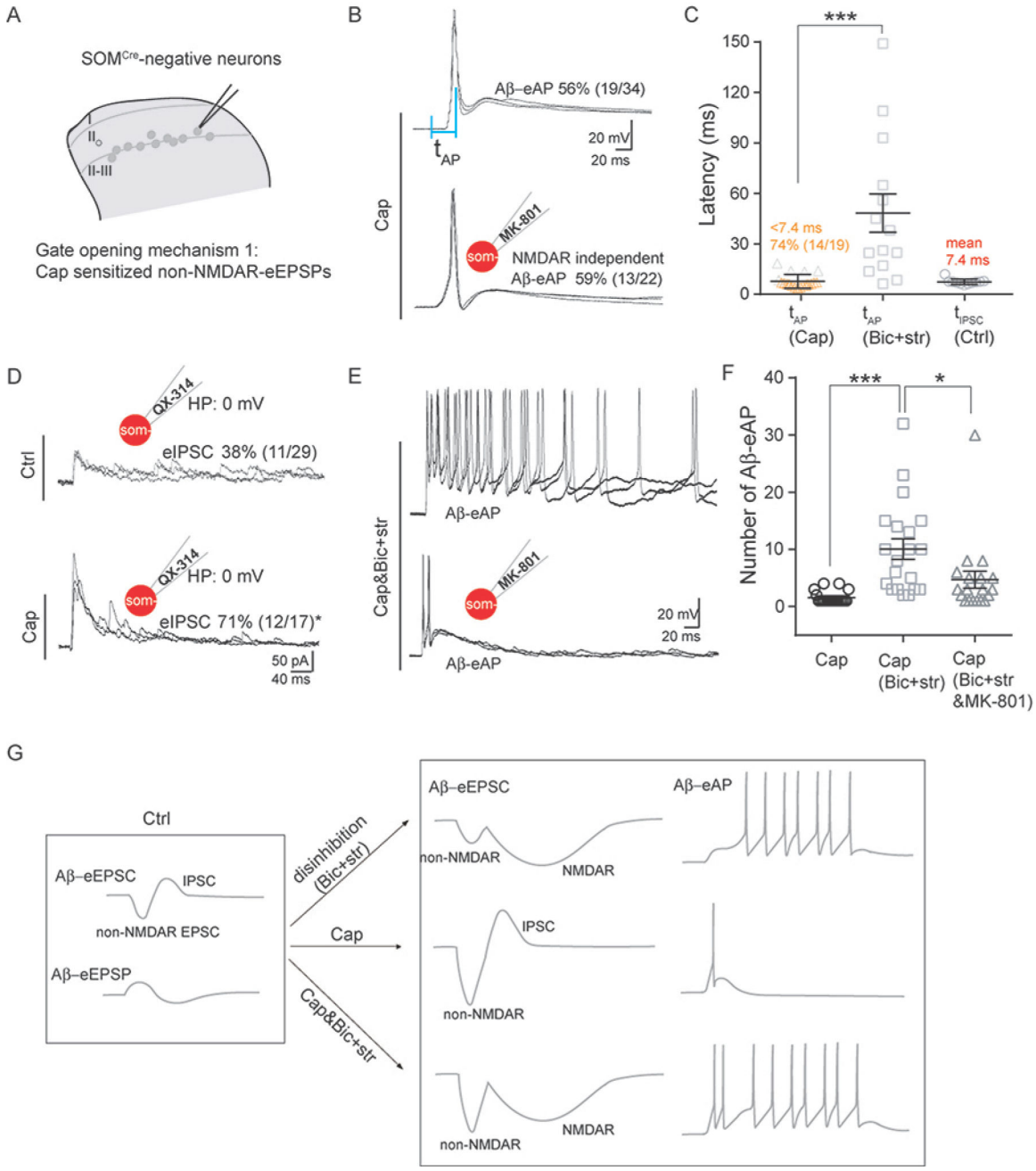

Figure 3. Capsaicin-induced sensitization and gate opening in SOM^{Cre}-negative neurons within $_{v}$II$_{i}$-$_{d}$III

(A) Schematics showing of recorded neurons and gate opening mechanism 1 induced by capsaicin.

(B) Representative traces of Aβ-evoked outputs in neurons within $_{v}$II$_{i}$-$_{d}$III from mice with capsaicin (“Cap”) treatment, with internal recording solution not containing (top) or containing 2 mM MK-801 (bottom). See Figure 2C for the latency defined by the intervals of two vertical blue lines.

(C) t_{AP} under the normal recording solution from Cap-injected mice ("t_{AP}, Cap") was shorter than t_{AP} under the disinhibition condition with Bic+str from naive mice ("t_{AP}, Bic +str"; two-tailed Student's unpaired test, ***$p < 0.001$). "t_{IPSC}, Ctrl" indicates t_{IPSC} under the normal recording solution in slice from naïve control mice.
(D) Representative traces of Aβ-eIPSCs in Ctrl mice versus Cap-injected mice, with 5 mM QX-314 included in the recording electrode. The percentage of neurons with Aβ-eIPSCs increased following Cap treatment (Chi-square test, *$p < 0.05$).
(E) Representative traces of Aβ-eAPs under the disinhibition condition ("Bic+str") or under disinhibition plus MK-801 ("Bic+str&MK-801") in slices prepared from Cap-injected mice.
(F) Comparison of the numbers of Aβ-eAPs in SOM^{Cre}-negative neurons from Cap-treated mice under the normal ("Cap"), disinhibition ("Cap, Bic+str"), or disinhibition plus MK-801 ("Cap, Bic+str&MK-801") conditions, showing significant difference (two-tailed Student's unpaired test, ***$p < 0.001$; *$p < 0.05$).
(G) Schematic summary of Aβ-induced inputs and outputs in neurons within $_{v}II_{i}$-$_{d}III$ under different situations.
All shown recordings (B, D, E) are composed of three traces at 0.033 Hz. Data are represented as means ± S.E.M. See also Figure S3.

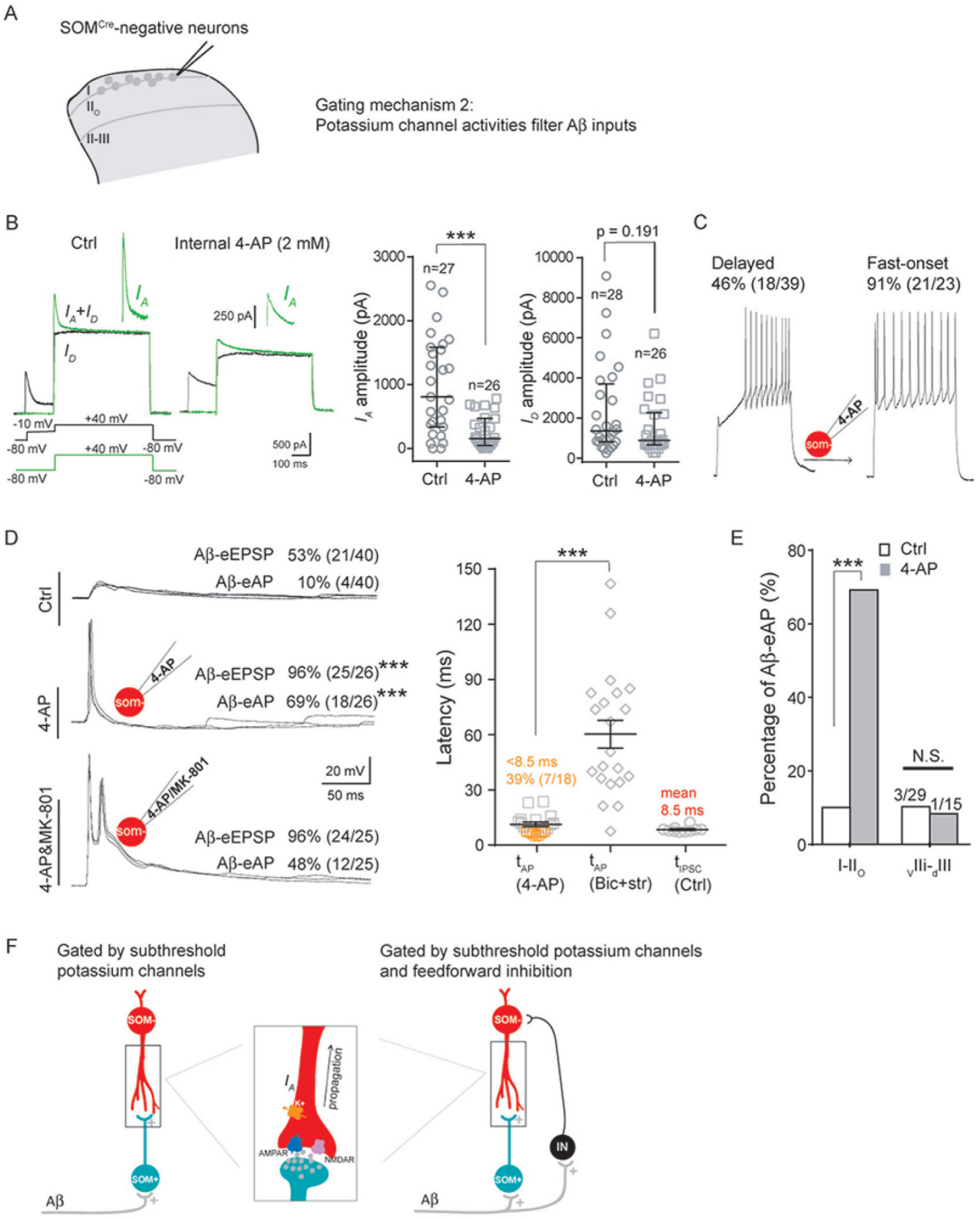

Figure 4. Potassium channel activities filter Aβ inputs

(A) Schematic showing of recorded SOM^{Cre}-negative neurons and the proposed gating mechanism 2.

(B) Left: the two-step protocol for I_A recording. The first step recorded both transient I_A plus persistent I_D potassium currents (green line); the second step recorded I_D after I_A inactivation. I_A was isolated by subtraction of the two traces. Right: reduction of the I_A amplitude by intracellular 4-AP (Mann-Whitney Rank Sum Test, ***p < 0.001), and a trend

of reduction in I_D without reaching significance (Mann-Whitney Rank Sum Test, "N.S.", p = 0.191).

(C) Transformation of delayed firing to fast-onset firing by intracellular 4-AP.

(D) Increased SOM^{Cre}-negative neurons with Aβ-eEPSP and Aβ-eAP after potassium channel blockage by 4-AP. Left: representative traces under normal internal solution ("Ctrl"), internal solution containing 4-AP ("4-AP") and internal solution containing 4-AP plus MK-801 ("4-AP&MK-801"). Right: significant difference in Aβ-eAP latencies with internal solution containing 4-AP ("t_{AP}, 4-AP") versus that under the disinhibition condition ("t_{AP}, Bic+stry"; two-tailed Student's unpaired test, ***p < 0.001). t_{IPSC} under the normal control recording condition was referred to as "t_{IPSC}, Ctrl".

(E) 4-AP treatment increased neurons with Aβ-eAPs in I-II_o (Chi-square test, ***p < 0.001), but not for neurons in $_vII_i$-$_dIII$ ("N.S", p = 1.000).

(F) Schematic showing of two mechanisms that prevent Aβ inputs from activating neurons in I-II_o. One is gated via electric filtering by subthreshold potassium channels only (left). The other is gated by subthreshold potassium channels plus feedforward activation of inhibitory neurons ("IN"). The rectangle in middle panel indicates the enlarged schematic of the synapse and dendrites, showing that following glutamatergic synaptic transmission, evoked depolarized potential along the dendrite to the soma can be modulated by the potassium channel activity including I_A.

The insets of schematic recording electrode show intracellular application of 4-AP (2 mM) or 4-AP plus MK-801 (2 mM). Recordings in B represent the average from five repeated traces. Recordings in C are the responses following 1 s, 150 pA current injection. Recordings in D are composed of three traces at 0.033 Hz. Data in B are represented as interquartile range (Q1–Q3 with median denoted in between). Data in D and E are represented as means ± S.E.M.. See also Figures S4 and S5.

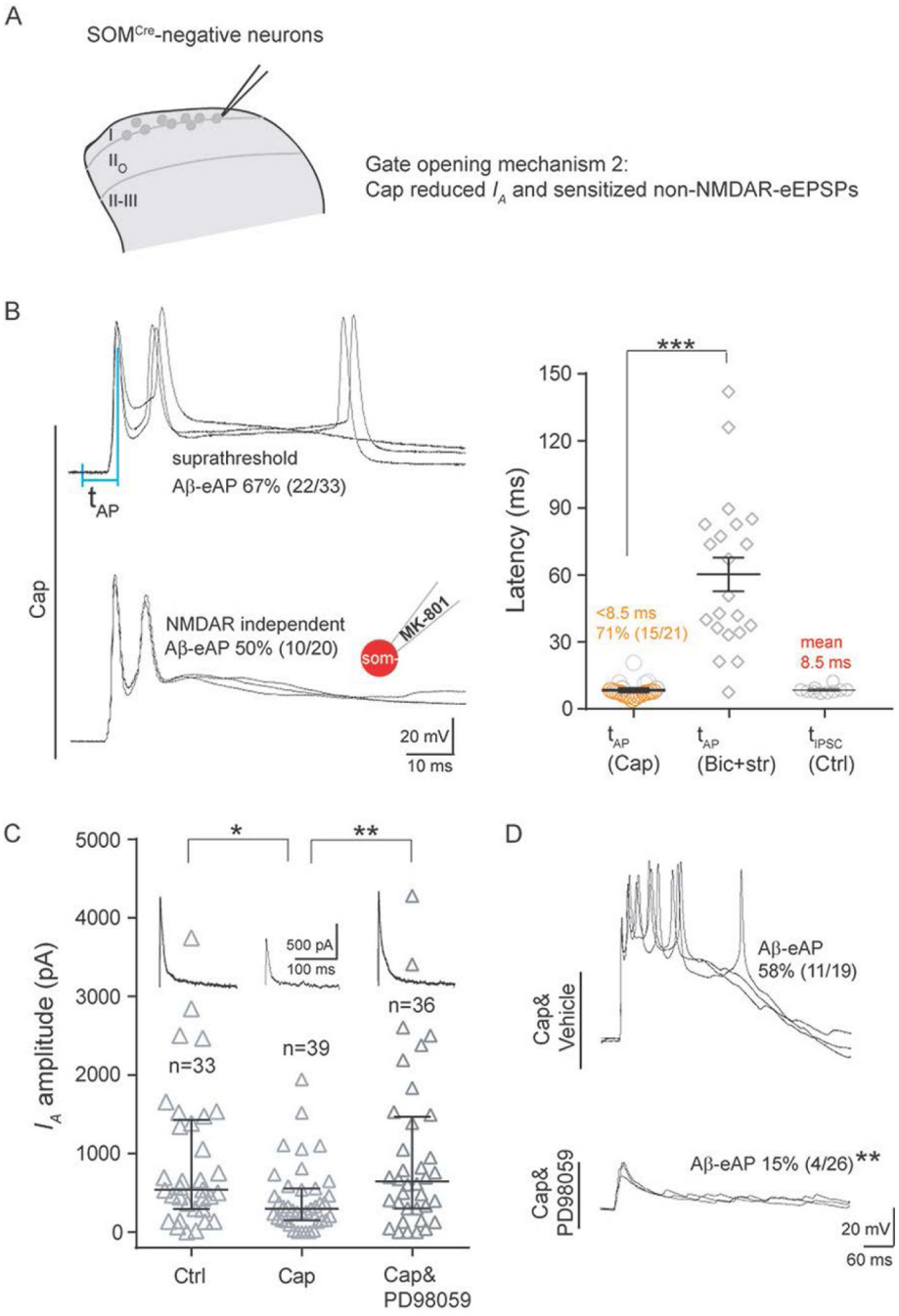

Figure 5. Capsaicin treatment reduced I_A in SOM^{Cre}-negative neurons within I-II$_0$

(A) Schematics showing of recorded neurons and our proposed gate opening mechanism 2 by capsaicin (“Cap”).

(B) Induction of NMDAR-independent Aβ-eAPs by Cap. Left: representative traces of Aβ-eAPs recorded from slices from Cap-treated mice, with internal solution not containing (“Cap”) or containing MK-801 (“Cap, MK-801)”. Right: latency comparison showing shorter latencies of Aβ-eAPs (t_{AP}), in Cap-injected mice under the normal ACSF condition (“t_{AP}, Cap”) in comparison with that in naive mice under the disinhibition condition (“t_{AP},

Bic+str"; two-tailed Student's unpaired test, ***p < 0.001). "t_{IPSC}, Ctrl" referred to as the latencies of IPSCs under the normal ACSF condition in naïve control mice. The inset of schematic recording electrode indicates intracellular application of MK-801 (2 mM). See Figure 2C for latencies defined by the intervals of two vertical blue lines.

(C) Comparison of I_A amplitudes in SOM^{Cre}-negative neurons from mice without Cap ("Ctrl") treatment, with Cap treatment ("Cap"), or with intrathecal injection of the MEK inhibitor PD98059 (10 μl, 0.5 μg, i.t.) at 0.5 hour before Cap treatment ("Cap&PD98059"). Note I_A reduction by Cap treatment (Mann-Whitney Rank Sum Test, *p < 0.05) and the reduction can be prevented by PD98059 treatment (Mann-Whitney Rank Sum Test, **p < 0.01).

(D) Abolishment of Cap-induced Aβ-eAPs by PD98059 treatment (10 μl, 0.5 μg, i.t) (Chi-square test, **p < 0.01). Representative traces of Aβ-evoked outputs in SOM^{Cre}-negative neurons within I-II_o with vehicle ("Cap&Vehicle") or with PD98059 ("Cap&PD98059") treatment.

Recordings in B and D are composed of three traces. Recordings in C represent the average from five repeated traces. Data in B are represented as means ± S.E.M. Data in C are represented as interquartile range (Q1–Q3 with median denoted in between). See also Figures S6–S8, and S10.

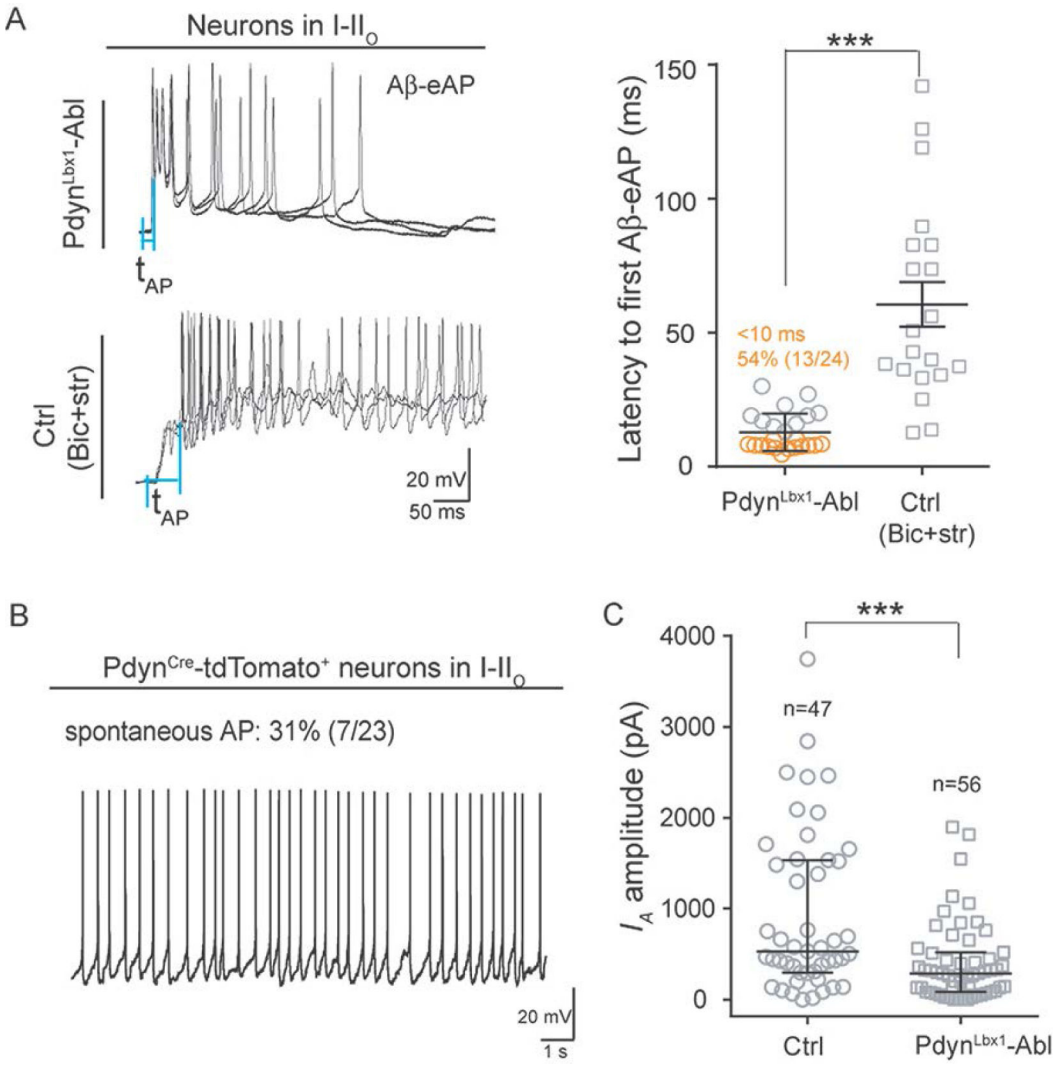

Figure 6. Requirement of Pdyn^{Cre}-derived neurons for establishing I_A currents in neurons within I-II$_o$

(A) Fast Aβ-eAPs in I-II$_o$ neurons in Pdyn^{Lbx1}-ablated mice ("Pdyn^{Lbx1}-Abl"). The latencies of Aβ-evoked firing in I-II$_o$ neurons of Pdyn^{Lbx1}-Abl mice under the normal ACSF condition is much shorter than the latencies seen in naïve control mice under the disinhibition condition ("Ctrl, Bic+str") (two-tailed Student's unpaired test, ***$p < 0.001$). See Figure 2C for latencies defined by the intervals of two vertical blue lines.

(B) Spontaneous firing of Pdyn^{Cre}-tdTomato$^+$ neurons in I-II$_o$.

(C) A reduction of I_A amplitudes in I-II$_o$ neurons in Pdyn^{Lbx1}-ablated mice in comparison with control ("Ctrl") littermates (Mann-Whitney Rank Sum Test, ***$p < 0.001$).

Recordings in A (left) are composed of three traces at 0.033 Hz. Data in A (right) are represented as means ± S.E.M. Data in C are represented as interquartile range (Q1–Q3 with median denoted in between). See also Figures S9–S11.